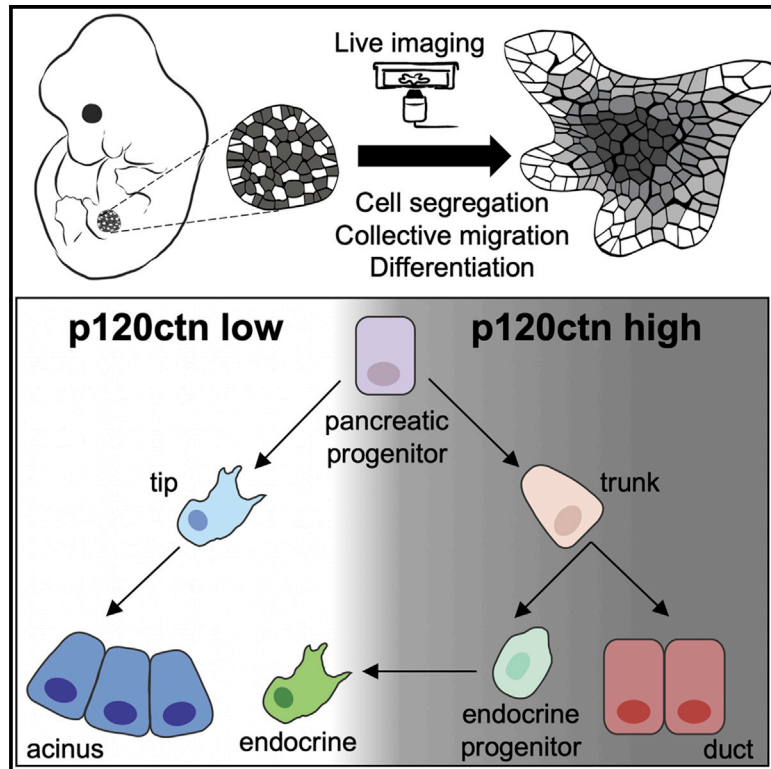


# Developmental Cell

## p120ctn-Mediated Organ Patterning Precedes and Determines Pancreatic Progenitor Fate

### Graphical Abstract



### Authors

Pia Nyeng, Silja Heilmann,  
Zarah M. Löf-Öhlin,  
Nina Fransén Pettersson,  
Florian Malte Hermann,  
Albert B. Reynolds, Henrik Semb

### Correspondence

pia.nyeng@sund.ku.dk (P.N.),  
semb@sund.ku.dk (H.S.)

### In Brief

Nyeng et al. use live imaging to demonstrate that differential p120-catenin expression segregates pancreatic progenitor cells into fate-determining niches by differential surface tension. While cells with low expression move to the periphery to become acinar cells, cells with high expression remain in the center to become duct and endocrine cells.

### Highlights

- p120ctn expression segregates pancreatic progenitors into fate determining niches
- p120ctn-low progenitors segregate into peripheral domains and form pro-acinar tips
- p120ctn-high progenitors remain in the trunk to become duct and endocrine cells
- p120ctn downregulation in endocrine cells drives delamination

# p120ctn-Mediated Organ Patterning Precedes and Determines Pancreatic Progenitor Fate

Pia Nyeng,<sup>1,\*</sup> Silja Heilmann,<sup>1</sup> Zarah M. Löf-Öhlin,<sup>1,5,6</sup> Nina Fransén Pettersson,<sup>2,7</sup> Florian Malte Hermann,<sup>1</sup> Albert B. Reynolds,<sup>3</sup> and Henrik Semb<sup>1,4,8,\*</sup>

<sup>1</sup>Novo Nordisk Foundation Center for Stem Cell Biology (Danstem), University of Copenhagen, 2200 Copenhagen N, Denmark

<sup>2</sup>Lund Stem Cell Center, Biomedical Center, 22184 Lund, Sweden

<sup>3</sup>Department of Cancer Biology, Vanderbilt University, Nashville, TN 37232, USA

<sup>4</sup>Institute of Translational Stem Cell Research, Helmholtz Zentrum München, Neuherberg, Germany

<sup>5</sup>Present address: Department for the Clinical Research Laboratory, Örebro University Hospital, Örebro 70362, Sweden

<sup>6</sup>Present address: Faculty of Medicine and Health, School of Medical Sciences, Örebro University, Örebro 70182, Sweden

<sup>7</sup>Present address: Department of Experimental Medical Sciences, Immunology, Lund University, Lund, 22100, Sweden

<sup>8</sup>Lead Contact

\*Correspondence: [pia.nyeng@sund.ku.dk](mailto:pia.nyeng@sund.ku.dk) (P.N.), [semb@sund.ku.dk](mailto:semb@sund.ku.dk) (H.S.)

<https://doi.org/10.1016/j.devcel.2019.02.005>

## SUMMARY

The mechanism of how organ shape emerges and specifies cell fate is not understood. Pancreatic duct and endocrine lineages arise in a spatially distinct domain from the acinar lineage. Whether these lineages are pre-determined or settle once these niches have been established remains unknown. Here, we reconcile these two apparently opposing models, demonstrating that pancreatic progenitors re-localize to establish the niche that will determine their ultimate fate. We identify a p120ctn-regulated mechanism for coordination of organ architecture and cellular fate mediated by differential E-cadherin based cell sorting. Reduced p120ctn expression is necessary and sufficient to re-localize a subset of progenitors to the peripheral tip domain, where they acquire an acinar fate. The same mechanism is used re-iteratively during endocrine specification, where it balances the choice between the alpha and beta cell fates. In conclusion, organ patterning is regulated by p120ctn-mediated cellular positioning, which precedes and determines pancreatic progenitor fate.

## INTRODUCTION

How organ shape and function emerge from the collective dynamic behavior and differentiation of individual cells is an intriguing basic biological question, which is also relevant for applications in cell replacement therapies. The close association between bio-architecture and cellular differentiation suggests that organ shape creates niches with specific signaling molecules and mechanical tension that direct cells toward their ultimate fate. Recent time-lapse imaging studies reveal significant cell rearrangements via active epithelial cell migration during organ morphogenesis (Ewald et al., 2008; Kuo and Krasnow, 2015; Shakya et al., 2005). This raises the question whether

fate decisions are determined by the final niche location, or whether progenitors are pre-destined to a particular fate prior to their movement into the niche. In support of the former, regulated movement of stem cells through the embryo to form a niche is crucial during establishment of the germline and the skeletal muscles (Laird et al., 2008). Here, we use the developing pancreas to investigate whether regulated movement of individual cells directs epithelial progenitor cells to and from their specifying niche(s) during organogenesis.

Pancreas development gives rise to a complex tubular network composed of peripheral tip and central trunk domains (Kesavan et al., 2009; Villasenor et al., 2010). Acinar cells appear at the tips, while the duct and endocrine lineages arise from the trunk (Zhou et al., 2007). Although the transcriptional networks underlying fate specification have been extensively mapped (MacDonald et al., 2010), not much is known about the mechanisms that regulate the spatial patterning. It is not known whether the cell lineages are pre-determined or become fixed once patterning has been established. Non-clonal lineage tracing of cells expressing the acinar differentiation determinant *Ptf1a* or the tip-marker *Carboxypeptidase A1* (*Cpa1*) has shown that these cells are multipotent up until tip-trunk establishment at E14.5 and acinar-committed thereafter (Pan et al., 2013), indicating that fate is secondary to niche establishment. However, clonal analysis has recently revealed an underlying heterogeneity in these lineages, with some unipotent acinar lineages present already at E11.5 (Larsen et al., 2017; Sznurkowska et al., 2018), suggesting specification prior to patterning.

Subsequent to tip-trunk patterning, the Neurogenin 3 (NEUROG3+) expressing pancreatic endocrine progenitors are specified in the trunk. These cells undergo a series of dynamic cell sorting and migration steps during their journey to become endocrine cells, including a reduction of their apical domain associated with increased expression of NEUROG3 and commitment toward the endocrine lineage (Löf-Öhlin et al., 2017). The NEUROG3+ cells are then believed to leave the trunk epithelium via an epithelial to mesenchymal transition (EMT)-like delamination process as they differentiate into endocrine cells and migrate through the mesenchyme to eventually form the islets of Langerhans (Cole et al., 2009; Gouzi et al., 2011; Puri and Hebrok, 2007; Rukstalis and Habener, 2007).

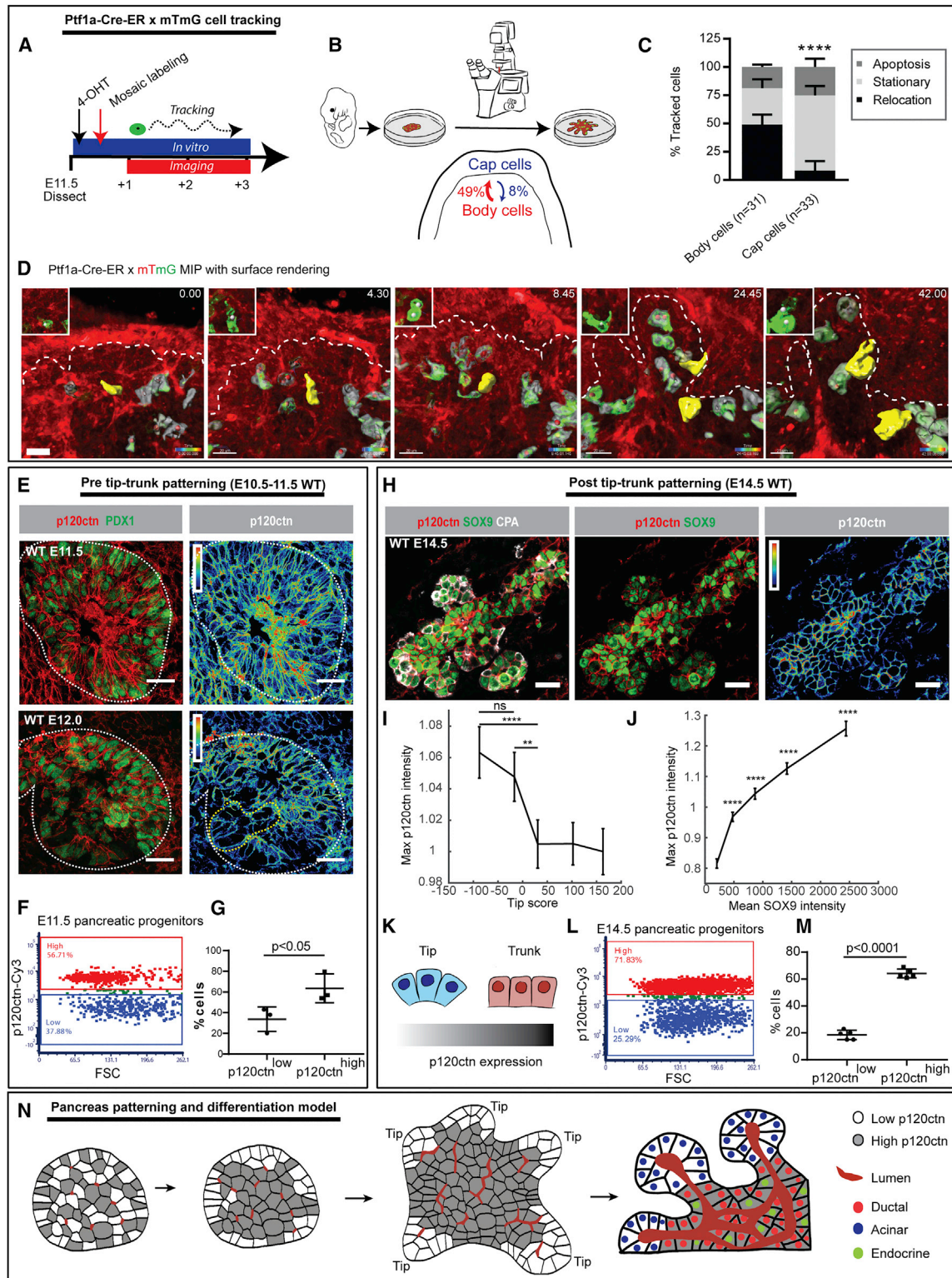


**Figure 1. Epithelial Progenitor Migration Drives Pancreatic Patterning**

(A and B) Schematic of the Ptf1a-Cre-ER live imaging experiment.

(C) Tracking in  $n = 3$  embryos. Mean  $\pm$  SEM. \*\*\*\* $p < 0.0001$  (chi-square test).

(legend continued on next page)

In this study, we demonstrate that pancreatic epithelial cells actively enter and exit specific instructive niches, as governed by p120-catenin (p120ctn) regulation, mediated by differential surface-tension-based cell sorting. p120ctn is an Armadillo-domain protein that functions as a master regulator of adherens junction (AJ) stability by binding to cadherins (Iretton et al., 2002) in addition to regulating the small Rho-GTPases (Noren et al., 2000). p120ctn has been implicated in regulation of migration and cell sorting in cancer and development (McCrea and Park, 2007; Peglion and Etienne-Manneville, 2013), including in the pancreas (Hamada et al., 2013; Hendley et al., 2016). Complete loss of the p120ctn coding gene *Ctnnd1* during pancreatic development interferes with branching and acinar differentiation (Hendley et al., 2015). To explore the role of p120ctn in pancreatic bio-architecture and cellular fate, we interfered with pancreatic p120ctn expression in either a mosaic, complete, or endocrine-restricted manner. We assessed the dynamics of cell shape, cell polarity, motility, and differentiation using a combination of 3D lineage tracing and live imaging. We demonstrate that mosaic ablation of *Ctnnd1* or *E-cadherin* (*Cdh1*) in a minority population of pancreatic progenitor cells is sufficient for inducing intraepithelial movement toward the periphery of the organ, thereby establishing a tip domain. Cell fate is dictated as a secondary consequence of this motility, as p120ctn or E-cadherin mosaicism is necessary and sufficient to drive acinar cell fate. We provide further support of p120ctn-mediated cellular rearrangements as a determinant of pancreatic progenitor fate using endocrine specific *Ctnnd1* ablation. Loss of p120ctn specifically from the endocrine lineage changes the balance between alpha and beta cell differentiation because of increased delamination. Based on these data, we propose that p120ctn-mediated cell dynamics is a determining factor linking organ patterning and cellular differentiation.

## RESULTS

### Epithelial Progenitor Migration Drives Pancreatic Patterning

To determine whether epithelial progenitors migrate during the transformation from a uniform pancreatic bud (E10.5) into a tree-like structure with defined tip and trunk domains

(E14.5–E18.5), we mosaically labeled *Ptf1a*-expressing progenitor cells in organotypic pancreatic cultures. E11.5 pancreatic buds from *Ptf1a*-Cre-ER (Pan et al., 2013), mTmG (Muzumdar et al., 2007) embryos were imaged over a 48 h period (Figure 1A). Cre-mediated recombination of the mTmG reporter allowed tracking of GFP+ clones among Tomato+ cells. GFP+ cells were evenly distributed in a mosaic fashion (Video S1; Figure S1A). We tracked peripherally located cap cells and internal body cells in a 48-h recording (Figure 1D; Video S1). Cap cells and body cells displayed highly different motility: 48% of the tracked body cell lineages had one or more progeny that relocated to the cap cell compartment, while only 8% of tracked cap cell lineages relocated to the body cell compartment (Figures 1B and 1C). Relocating cells extended protrusions, indicative of active intraepithelial migration. There was no difference in cell division or apoptosis (Figure S1B). A longer tracking duration compared to a previous study (Shih et al., 2016) most likely explains the significant relocation between compartments. We conclude that there is considerable cell relocation from the central compartment toward the periphery during tip formation.

### Differential p120ctn Expression Correlates with Tip-Trunk Patterning

According to the differential adhesion hypothesis (DAH), a population of cells with different adhesive properties will spontaneously tend to sort in order to maximize adhesive bonding (Foty and Steinberg, 2005). The DAH has later been extended to include a combination of adhesion and cortical tension, which generates differential surface tension (Brodland, 2002; Harris, 1976; Manning et al., 2010). Since p120ctn regulates both adhesion (via Cadherins) and cortical tension (via small Rho-GTPases), we investigated whether differential expression of p120ctn could be the driving force behind the epithelial cell relocation.

p120ctn protein is expressed at the cell membranes (but never in the nucleus) of the pancreatic epithelial and mesenchymal cells (Figure 1E) (Hendley et al., 2015). As the pancreatic epithelium becomes progressively organized into a pseudo-stratified and tip-trunk patterned epithelium (from E13.5), the expression of p120ctn becomes restricted to the lateral membranes and co-localizes with E-cadherin (E-cad) and Beta-catenin

(D) Examples of maximum intensity projections (MIPs) from one time-lapse experiment showing a body cell clone (yellow) giving rise to cap and body cell progeny. Time is specified in h and min. Tomato, red; GFP, green. Surface rendering of GFP signal in gray or yellow (yellow representing one clone). Spheres were used for tracking. Insert: raw image for yellow clone. White stippled line: epithelial/mesenchymal boundary based on DIC images (not shown). Scale bar, 20  $\mu$ m.

(E) High-resolution confocal images from E11.5 and E12.0 WT pancreatic tissue. Left, p120ctn and PDX1; right, p120ctn intensity lookup table (LUT) as specified in insert. Scale bar, 20  $\mu$ m.

(F) Representative FACS plot of p120ctn-Cy3 intensity within the pancreatic progenitor population of one E11.5 dorsal pancreas.

(G) p120ctn<sup>LOW</sup> and p120ctn<sup>HIGH</sup> fractions in n = 3 E11.5 embryos. Mean  $\pm$  SEM. p value was calculated using a two-tailed t test.

(H) Confocal images from E14.5 WT pancreatic tissue. Left to right: p120ctn, SOX9, and CPA1; p120ctn and SOX9; p120ctn intensity LUT. Scale bar, 20  $\mu$ m.

(I and J) Automated quantification of normalized max p120ctn intensity in linescan between two cell nuclei. Median  $\pm$  confidence interval. ns, not significant. \*\*p < 0.01, \*\*\*\*p < 0.0001 (Wilcoxon signed-rank test).

(I) p120ctn membrane intensity versus tip score. n = 3,305–3,400 cell pairs per class (4 embryos).

(J) p120ctn membrane intensity versus mean nuclear SOX9 intensity. n = 1,000–2000 cell pairs per class (4 embryos).

(K) Schematic showing the gradient in p120ctn membrane expression.

(L) FACS plot of p120ctn-Cy3 intensity within the pancreatic progenitor population of one E14.5 dorsal pancreas.

(M) p120ctn<sup>LOW</sup> and p120ctn<sup>HIGH</sup> fractions in n = 5 E14.5 embryos. Mean  $\pm$  SEM. p value was calculated using a two-tailed t test.

(N) Drawing illustrating the central hypothesis: An initial mixed population of p120ctn-high and -low cells sort-based on differential surface tension in a minority population to form discrete p120ctn-low domains at the periphery. These domains give rise to patterning into p120ctn-high trunk epithelium-containing endocrine and ductal cells and p120ctn-low tip epithelium consisting of acinar cells.

See also Figures S1 and S7; Video S1.

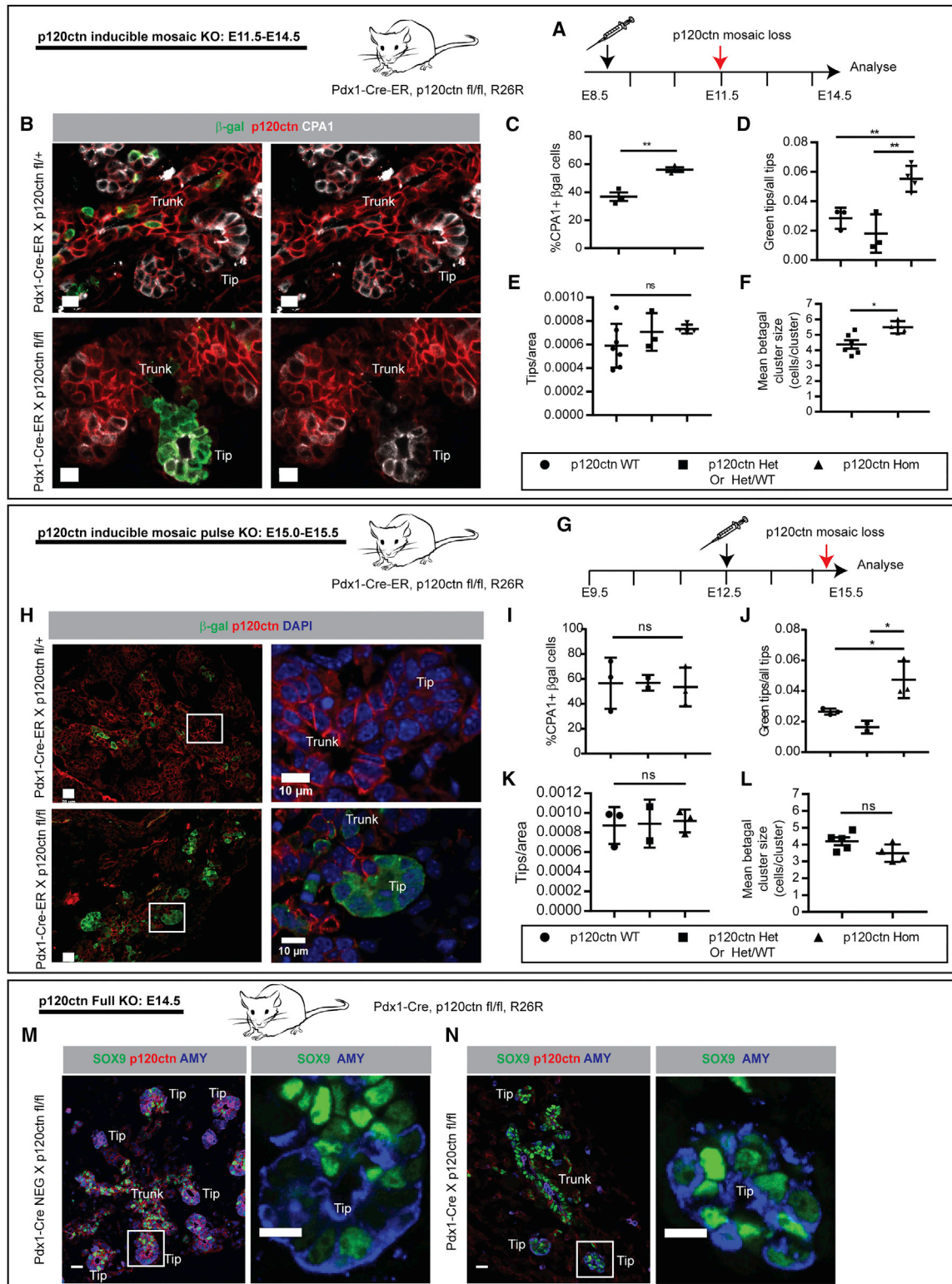


**Figure 2. Mosaic Expression of p120ctn Is Sufficient and Necessary for Tip-Trunk Patterning**

(A-F) Inducible mosaic p120ctn ablation from E11.5 to E14.5 with Pdx1-Cre-ER.

(A) Schematic of the experiment.

(B) IF staining for  $\beta$ -gal, p120ctn, and CPA1 in HET (Pdx1-Cre-ER  $\times$  p120ctn fl/+) and HOM KO (Pdx1-Cre-ER  $\times$  p120ctn fl/fl) pancreas. Scale bar, 10  $\mu$ m.

(C-F) Quantification of IF staining. Mean  $\pm$  SEM. ns, not significant, \* $p < 0.05$ , \*\* $p < 0.01$  (two-tailed t test).

(legend continued on next page)

(Beta-cat) (Figures S1C, 5B, 5D, and 7E). Heterogeneous expression levels of p120ctn were observed by high-resolution confocal analysis in the unpatterned E11.5 pancreas (Figure 1E and E-cad in Figure S1C). Interestingly, streaks of cells with low p120ctn expression (p120ctn<sup>LOW</sup>) were seen at E12.0 (yellow stippled line in Figure 1E). Fluorescence-activated cell sorting (FACS) analysis of E11.5 pancreata from E-cad-CFP (Snippert et al., 2010) × Pdx1-GFP (Holland et al., 2006) mice confirmed that pancreatic progenitor cells can be divided into two distinct populations based on p120ctn expression (Figures 1F, 1G, and S1F–S1H). Although E-cad expression was heterogeneous and most E-cad<sup>LOW</sup> cells (red box in Figure S1H) were p120ctn<sup>LOW</sup>, not all p120ctn<sup>LOW</sup> cells were E-cad<sup>LOW</sup>. We ascribe this to detection of non-membrane-located E-cad-CFP.

When tip-trunk patterning is almost complete, p120ctn become enriched in the central trunk cells (Figure 1H). Trunk-to-tip intensity profiles (Figures S1D and S1E) showed a declining expression of SOX9 (duct marker) and p120ctn, while CPA1 (tip marker) increased. This observation was verified using a new method for automatic scoring of the position of a cell relative to the tip or trunk domains based on geometric features (tip-score, Figure S7). An increased tip score is associated with reduced expression of membrane p120ctn (Figure 1I). Further, automatic quantification showed a positive correlation between SOX9 and membrane p120ctn expression (Figure 1J). FACS analysis of E14.5 pancreata showed distinct populations of p120ctn-high and low cells (Figures 1L, 1M, and S1I). In order to probe whether the phenomenon is preserved in humans, we stained for p120ctn (CTNND1), SOX9, and the tip markers GATA4 and MIST1 (BHLHA15) in human fetal 10.5 and 12.5 weeks post-conception (wpc) pancreatic samples. A p120ctn expression gradient could be observed in some tip-trunk units (Figures S5L and S5M, profile I) but not consistently (Figure S5M, profile II). We believe this is because, as evident by SOX9 and MIST1 expression, human tip-trunk patterning is not complete at this time (Jennings et al., 2013).

We conclude that p120ctn is expressed heterogeneously in the unpatterned pancreas and in a trunk-tip gradient in the patterned epithelium (Figure 1K). Based on these results, we hypothesize that differential expression of p120ctn leads to differential surface tension and increased motility of p120ctn<sup>LOW</sup> cells toward the peripheral region (tips) of the organ (Figure 1N). Surface tension models predict that a mixture of low- and high-

adhesion cells would lead to sorting of low-adhesion cells to the entire outside surface or to discrete clusters on the surface, depending on their affinity for the outside (ECM) and the fraction of adhesion-low and high cells (Hutson et al., 2008). Since we observe only 20%–40% p120ctn<sup>LOW</sup> cells, this is compatible with sorting to discrete domains that serve as initiation sites for tip formation. If the tip niche determines cellular fate, such a scenario would eventually be predicted to lead to an enrichment of acinar differentiation in p120ctn<sup>LOW</sup> cells, while p120ctn<sup>HIGH</sup> cells would remain in the middle of the organ and therefore differentiate toward the ductal or endocrine lineages (Figure 1N).

### Mosaic Expression of p120ctn Is Sufficient and Necessary for Tip-Trunk Patterning

To test whether the heterogeneous expression of p120ctn drives patterning and differentiation, we analyzed the consequence of mosaic ablation of *Ctnnd1* (p120ctn) in pancreatic progenitor cells *in vivo*. To ablate *Ctnnd1* in pancreatic progenitors, p120ctn fl/fl mice (Davis and Reynolds, 2006) were intercrossed with Pdx1-Cre-ER mice (Gu et al., 2002) to obtain p120ctn inducible mosaic knockout (KO), or with Pdx1-Cre mice (Gu et al., 2002) to obtain p120ctn complete pancreatic KO. We used R26R mice (Soriano, 1999) as a reporter for Cre expression. However, recombination of the *Ctnnd1* locus was less efficient compared to the *Rosa26* locus (Figure S2B).

Loss of p120ctn protein occurred between the second and the third day post injection (Figures S2I–S2K). To induce loss of p120ctn at the primary transition (E11.5), tamoxifen was injected at E8.5 (Figure 2A). 3 days after p120ctn loss, p120ctn KO cells were enriched in the peripheral CPA1<sup>+</sup> tips as compared to recombinant cells from p120ctn heterozygous (HET) littermates (Figures 2B and 2C). Strikingly, some tips consisted only of p120ctn KO cells (Figure 2B). Manual counting of the number of tips with maximum one beta-galactosidase (βgal) negative cell in a continuous tip epithelium (“green tips,” Figure 2D) showed that they were two times more frequent in homozygous (HOM) KO littermates (6%) compared to wild-type (WT) and HET littermates. Moreover, % green tips and cluster size were higher in all HOM KO embryos irrespective of recombination frequency (Figures S2C and S2D). Consistently, automated analysis identified increased clustering of βgal<sup>+</sup> cells in HOM KO embryos (Figure 2F). This phenomenon was not due to an increase of βgal<sup>+</sup> cells in mosaic HOM KO embryos, as βgal<sup>+</sup> cells/area was

(C) CPA1<sup>+</sup>;β-gal<sup>+</sup>/β-gal<sup>+</sup> cells in p120ctn HET (n = 3 embryos) and HOM KO (n = 3 embryos).

(D) % tips with ≤ 1 βgal<sup>-</sup> cell in a continuous tip epithelium (“green tips”) in p120ctn WT (n = 3 embryos), HET (n = 3 embryos), and HOM KO (n = 4 embryos).

(E) Number of tips per E-cad area in p120ctn WT (n = 3 embryos), HET (n = 3 embryos), and HOM KO (n = 4 embryos).

(F) Automated quantification of mean cell number per β-gal<sup>+</sup> cluster in WT/HET (n = 6 embryos) and HOM KO (n = 4 embryos).

(G–L) Inducible mosaic p120ctn ablation from E15.0 to E15.5 with Pdx1-Cre-ER.

(G) Schematic of the experiment.

(H) IF staining for β-gal, p120ctn, and DAPI in HET (Pdx1-Cre-ER × p120ctn fl/+) and HOM KO (Pdx1-Cre-ER × p120ctn fl/fl) pancreas. Scale bars, 20 μm (left) and 10 μm (right).

(I–L) Mean ± SEM. ns, not significant, \*p < 0.05 (two-tailed t test).

(I) CPA1<sup>+</sup>;β-gal<sup>+</sup>/β-gal<sup>+</sup> cells in p120ctn WT (n = 3), HET (n = 2), and HOM KO (n = 3) embryos.

(J) % green tips in p120ctn WT (n = 3), HET (n = 2), and HOM KO (n = 3) embryos.

(K) Number of tips per E-cad area in p120ctn WT (n = 3), HET (n = 3), and HOM KO (n = 4) embryos.

(L) Automated quantification of mean cell number per βgal<sup>+</sup> cluster in WT/HET (n = 5) and HOM KO (n = 4) embryos.

(M and N) Pancreatic full epithelial p120ctn ablation with Pdx1-Cre. Staining for SOX9, p120ctn, and AMY in (M) WT (Pdx1-Cre<sup>NEG</sup> × p120ctn fl/fl) and (N) HOM KO (Pdx1-Cre × p120ctn fl/fl) pancreas. Scale bar, 10 μm.

See also Figure S2.

unchanged (Figure S2A). The total number of tips per epithelial area remained constant (Figure 2E), suggesting that the pancreas is able to independently regulate the number of tips.

To exclude the possibility that p120ctn loss leads to precocious differentiation prior to tip re-location, KO cells were analyzed shortly following p120ctn loss. Mosaic pulse KO was performed by injection of tamoxifen at E12.5 and analysis at E14.5 and E15.5. At E14.5, p120ctn levels were unchanged, while 10% of  $\beta\text{gal}^+$  cells had lowered p120ctn levels at E15.5 (Figures S2F and S2K). Consistent with previous results, p120ctn KO cells were enriched in the peripheral tips at E15.5 (Figures 2H and 2J) irrespective of recombination frequency (Figures S2E and S2G). Again, the total number of tips per epithelial area remained constant (Figure 2K). p120ctn KO cells in the pulse experiment showed no increase in CPA1 expression or cell clustering (Figures 2I, 2L, and S2H). These results demonstrate that p120ctn KO cells relocate toward the peripheral tip prior to induction of tip markers and cell clustering. Thus, increased acinar differentiation upon prolonged p120ctn loss is the result of relocation to the tip niche.

Disruption of the p120ctn gradient by complete ablation of p120ctn in the pancreas (Pdx1-Cre, p120ctn fl/fl, R26R; hereafter named p120ctn FULL KO) has previously been shown to lead to defects in acinar differentiation and branching (Hendley et al., 2015). In order to determine if p120ctn is necessary for tip-trunk patterning, we analyzed the p120ctn FULL KO for Amylase (AMY, an acinar marker), SOX9, Mucin1 (MUC1, a duct marker), and p120ctn expression at E14.5 (Figures 2M and 2N) and E18.5 (Figure S2L). We observed aberrant SOX9 expression in AMY<sup>+</sup> tips at both stages, indicative of failure to segregate the tip domain. At E14.5, there were fewer AMY<sup>+</sup> tips than normal (Figures 2M and 2N). Although a tendency toward decreased AMY and increased SOX9 area was observed, AMY and SOX9 expression was not significantly changed at E18.5 and P0 (Figures S2L–S2N). The tip-trunk patterning defect was corroborated by transmission electron microscopy (TEM) analysis of E18.5 p120ctn FULL KO pancreata, where intermingling of vesicle-containing acinar-like cells and ductal cells were found in peripheral cystic structures (Figure S2M). Importantly, acinar cells were never detected in the trunk region, demonstrating that p120ctn depletion cannot drive acinar differentiation outside of the tip niche.

In conclusion, our results show that differential expression of p120ctn is both sufficient and necessary for tip formation and that acinar differentiation is a secondary consequence of relocation of p120ctn<sup>LOW</sup> cells.

### Differential Expression of p120ctn Triggers Tip Formation by Collective Cell Migration

Live imaging of organotypic explants was carried out to analyze the effect of p120ctn mosaic KO on cellular dynamics. To circumvent the problem with inefficient Pdx1-Cre-ER-mediated recombination at the *Ctnd1* locus, we took advantage of low Cre-expression in the offspring from select Pdx1-Cre males and established KO models with mosaic ( $\leq 30\%$ ) recombination efficiency (Pdx1-Cre-LOW p120ctn mosaic KO) (Figure S3A). E12.5 pancreatic dorsal buds from Pdx1-Cre-LOW, p120ctn fl/fl, mTmG embryos, and p120ctn HET littermates were imaged for up to 48 h (Figure 3A). Post-imaging analysis demonstrated

normal growth, differentiation, and branching of WT, HET, and HOM KO embryos, while Pdx1-Cre-FULL embryos showed the published (Hendley et al., 2015) cystic phenotype (Figures S3A and S3B).

While no cell sorting was observed in Pdx1-Cre-LOW, p120ctn fl/+, mTmG control pancreata (n = 3) (Figure 3C; Video S2), Pdx1-Cre-LOW, p120ctn fl/fl, mTmG pancreata showed sorting into GFP+ p120ctn KO cells and Tomato+ WT cells (Figure 3D; Video S3, observed in n = 4 out of 5 KO embryos). p120ctn KO cells sent out filopodia and lamellipodia in a directional manner (see cell marked by arrow in Figure 3D). GFP+ cells in control embryos displayed the same dynamics in cell shape but lacked protrusion directionality (see cell marked by arrow in Figure 3C). Once p120ctn KO cells were sorted to the peripheral epithelium, we observed invasive, collective cell migration of p120ctn KO cells into the mesenchyme with very active filopodia and lamellipodia in clearly polarized leading cells (see leading cell (\*) at 7.00–12.00 h in Figure 3E). This behavior resulted in formation of tips consisting only of p120ctn KO cells (Figures 3E and S3C; Videos S4 and S5, n = 5 out of 5 KO embryos). Tips consisting of only GFP+ cells were never observed in HET littermates (n = 3). Notably, changes in cell shape and motility were similar to those observed during formation of normal tips in E11.5 HET pancreatic cultures (Figure S3D; Video S6), suggesting that collective cell migration also occurs during normal pancreatic morphogenesis. This is consistent with our observation that streaks of p120ctn low cells form in WT embryos at E11.5 (Figure 1E).

### p120ctn-Deficient Cells Ablated after Tip-Trunk Patterning Become Specified into the Acinar Lineage

Loss of p120ctn in the entire pancreas in the p120ctn FULL KO (Pdx1-Cre, p120ctn fl/fl, R26R) did not interfere notably with endocrinogenesis or ductal differentiation (Figures 2M, 2N, S2J, and S4T) (Hendley et al., 2015). However, induced mosaic loss of p120ctn (Pdx1-Cre-ER, p120ctn fl/fl, R26R) at E14.5 (Figure 4A) directed the majority of KO cells to an acinar fate (AMY+; Figures 4E and 4J) at the expense of beta cell (INS+), alpha cell (GCG+), and ductal cell (SOX9+) fates (Figures 4B–4D and 4G–4I). p120ctn does not affect the differentiation capacity of neighboring WT cells (Figures S4A–S4D). Moreover, we found no evidence of selective loss or expansion of the p120ctn KO population (Figures S4E and S4F). Thus, it is not the mere loss of p120ctn itself that causes the failure to form endocrine and ductal cells. These results demonstrate that p120ctn KO cells are shunted into an acinar fate after they relocate to the periphery to form tip domains (Figures 4F and 4K) and that this capacity is retained post patterning.

### Endocrine Delamination and Differentiation Is Associated with Decreased Expression of p120ctn

We next asked whether reduced expression of p120ctn also functions in the dynamic process where endocrine cells leave the trunk niche. p120ctn protein expression analysis demonstrated a striking change during endocrinogenesis. At E14.5, NEUROG3+ endocrine progenitors situated in the duct express p120ctn at the membrane (Figure 5A), similar to their neighboring bi-potent progenitors. However, p120ctn protein was downregulated in all INS+ cells associated with the duct (Figures 5B and 5C). E-cad (Figures 5B, S5A, and S5B) and Beta-cat (Figure 5D)

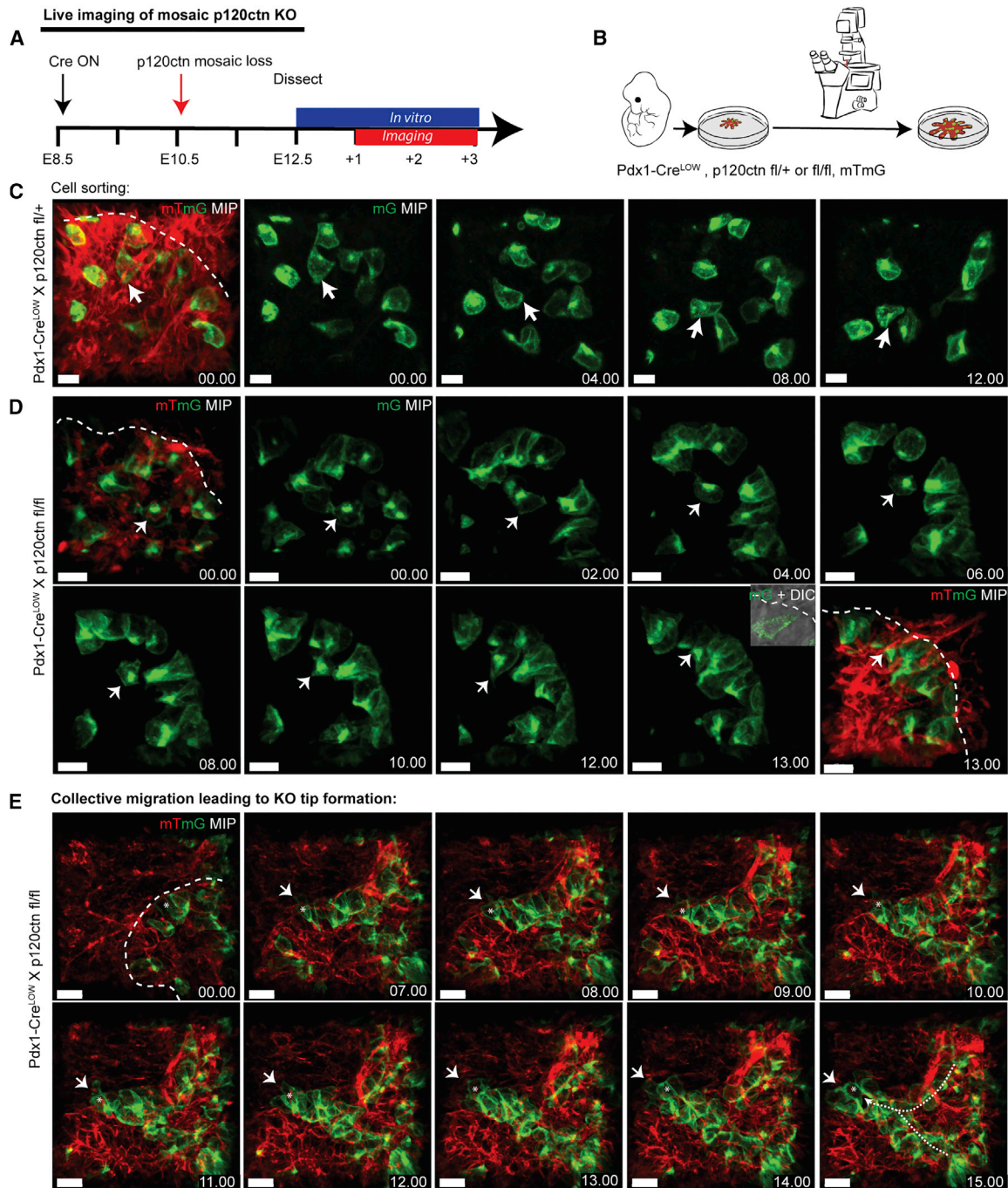


**Figure 3. Differential Expression of p120ctn Triggers Tip Formation by Collective Cell Migration**

(A and B) Schematic of the Pdx1-Cre<sup>LOW</sup> × p120ctn fl/fl or p120ctn fl/+ live imaging experiments.

(C–E) Examples of maximum intensity projections (MIPs) of Tomato (red) and GFP (green) signal. Time is specified in h and min. White stippled line: epithelial/mesenchymal boundary based on DIC images (not shown). Scale bars, 10 μm in (C) and (D), 15 μm in (E).

(C) GFP<sup>+</sup> cells in HET littermate dynamically change shape and send out exploratory filopodia, but with minor cell displacement. Arrow: one cell marked at different intervals. n = 3 embryos.

(D) GFP<sup>+</sup> cells in HOM KO explant dynamically change shape and send out filopodia and lamellipodia in the general direction of movement. Arrow: one cell marked at different intervals. Clustering observed in n = 4/5 embryos.

(E) GFP<sup>+</sup> cells in HOM KO explant cluster at the interface between the epithelium and mesenchyme. A leader cell (\*) sends filopodia (arrows) into the mesenchymal compartment and initiates collective migration of GFP<sup>+</sup> cells to form a tip-like protrusion. Observed in n = 5/5 embryos.

See also [Figure S3](#) and [Videos S2, S3, S4, S5, and S6](#).

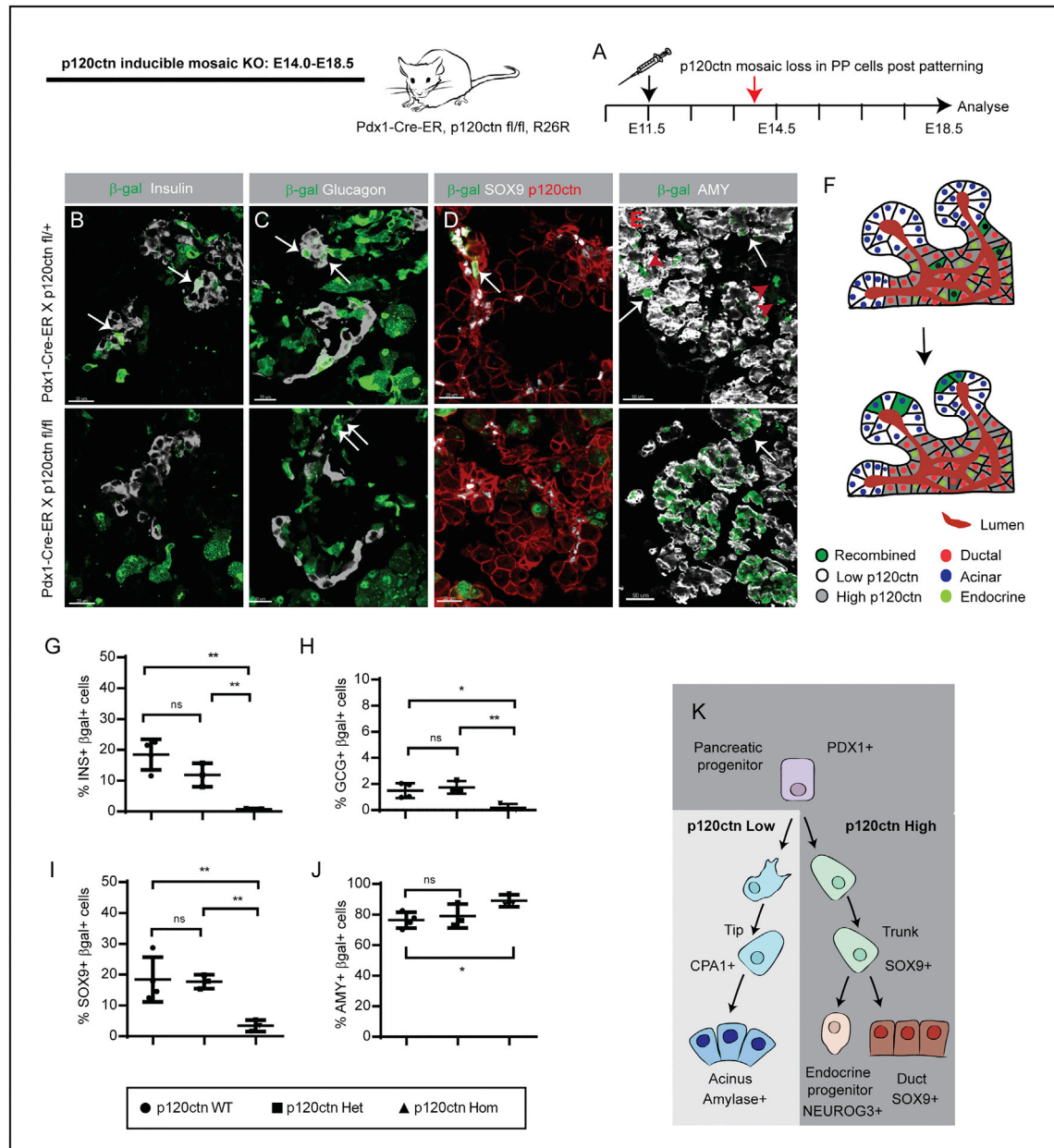


**Figure 4. p120ctn-Deficient Cells Ablated after Tip-Trunk Patterning Become Specified into the Acinar Lineage**

(A–J) Inducible and mosaic p120ctn ablation from E14.0 to E18.5 with Pdx1-Cre-ER.

(A) Schematic of the experiment.

(A–E) IF staining for  $\beta$ -gal, (p120ctn) and INS (A), GCG (B), SOX9 and p120ctn (D), and AMY (E) in HET and HOM KO pancreas. Scale bars, 20  $\mu$ m in (A)–(D) and in 50  $\mu$ m (E). Arrows:  $\beta$ gal<sup>+</sup>, marker<sup>+</sup> cells. Red arrowhead:  $\beta$ gal<sup>+</sup>, marker<sup>-</sup> cells.

(F) Drawing showing randomly p120ctn-ablated cells in the patterned pancreas relocating to the tip region and attaining an exocrine fate.

(G–J) Quantification of IF staining. Mean  $\pm$  SEM. ns, not significant, \* $p < 0.05$ , \*\* $p < 0.01$  (two-tailed t test). p120ctn WT (n = 4), HET (n = 3), and HOM KO (n = 3) embryos.

(G) Endocrine INS<sup>+</sup>;  $\beta$ gal<sup>+</sup>/ $\beta$ gal<sup>+</sup> cells.

(H) Endocrine GCG<sup>+</sup>;  $\beta$ gal<sup>+</sup>/ $\beta$ gal<sup>+</sup> cells.

(I) Ductal SOX9<sup>+</sup>;  $\beta$ gal<sup>+</sup>/ $\beta$ gal<sup>+</sup> cells.

(J) Acinar AMY<sup>+</sup>;  $\beta$ gal<sup>+</sup>/ $\beta$ gal<sup>+</sup> cells.

(K) Model of p120ctn regulation and cell fate. p120ctn<sup>LOW</sup> cells move to a peripheral position and are shunted into an exocrine fate. p120ctn<sup>HIGH</sup> cells remain in the trunk and become either endocrine or ductal cells.

See Figure S4.

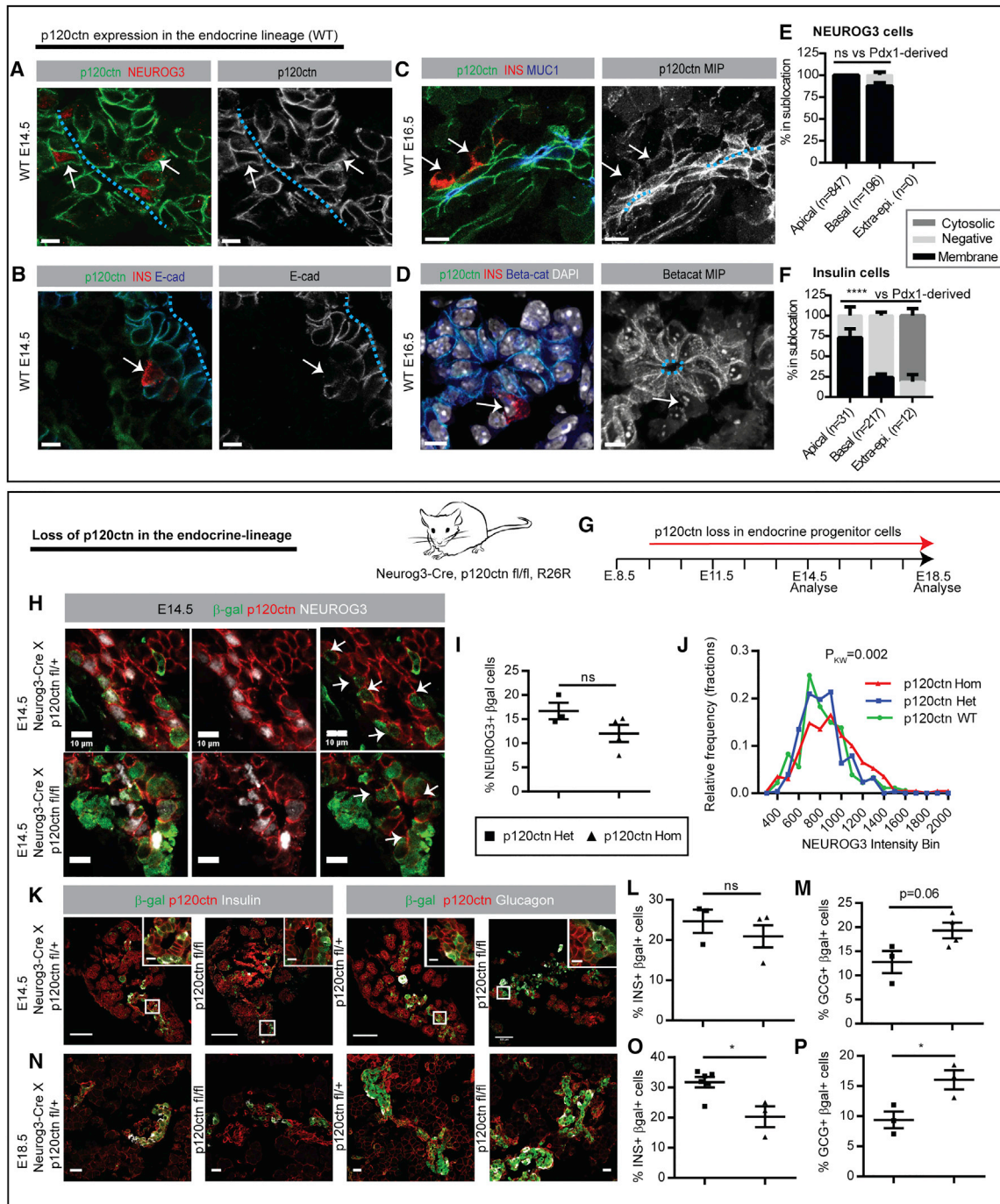


**Figure 5. Endocrine Delamination Is Associated with Decreased Expression of p120ctn and Ablation of p120ctn in Endocrine Progenitors Enhances Delamination and Alpha Cell Differentiation**

(A–D) Confocal images of IF stained WT pancreatic ducts.

(A) p120ctn and NEUROG3 at E14.5.

(B) p120ctn, INS, E-cad at E14.5.

(C) p120ctn, INS, MUC1 (left), and maximum intensity projection (MIP) of p120ctn (right) at E16.5.

(D) p120ctn, INS, β-cat, DAPI (left), and MIP of β-cat (right) at E16.5.

Scale bars, 7 μm in (A), (B), and (D) and 10 μm in (C). Arrows: NEUROG3/INS<sup>+</sup> cells. Blue stippled line: lumen of the pancreatic duct.

(E and F) Quantification of p120ctn expression relative to cell position in 3D IF stained E14.5 pancreas.

(E) NEUROG3<sup>+</sup> cells.

(F) INS<sup>+</sup> cells. Mean ± SD of n = 3 WT embryos. p values (chi-square test): NEUROG3 (Figure 5E) versus Pdx1-derived (Figure S5D): p = 0.07 excl. extraepithelial fraction, \*\*\*\*p < 0.0001 incl. extraepithelial fraction. INS (Figure 5F) versus Pdx1-derived: \*\*\*\*p < 0.0001 incl. and excl. extraepithelial fraction.

(legend continued on next page)

showed a similar expression pattern. To relate p120ctn expression to differentiation and cell position in the epithelium in a quantitative manner, we performed lineage tracing of all epithelial-derived pancreatic cells in 3D reconstructions of thick sections from Pdx1-Cre, R26R mice. 100% of epithelial cells with apical polarization ( $\beta$ gal+ and MUC1+) expressed p120ctn at the membrane. 93% of epithelial cells in the outer layer ( $\beta$ gal+ and pan-Laminin+ (LAM+), MUC1-) expressed p120ctn at the membrane, and 90% of  $\beta$ gal+ cells without contact to the epithelium had cytosolic localization of p120ctn (Figure S5D). While the expression of p120ctn was similar in NEUROG3+ and  $\beta$ gal+ cells (Figure 5E), INS+ cells were more frequently associated with loss of p120ctn expression (p120ctn-), especially in the basal position (76%) (Figure 5F). This p120ctn expression pattern is preserved in the human pancreas, as NEUROG3+ cells express p120ctn, while INS+ cells do not (Figure S5F).

qPCR analysis of sorted NEUROG3+ cells from E15.5 embryos confirmed that NEUROG3+ cells express *Ctnnd1* mRNA (Figure S5C). As NEUROG3<sup>HIGH</sup> cells are mainly situated with the cell body at an outer position in the epithelium (Löff-Öhlin et al., 2017), we analyzed whether *Ctnnd1* differed between NEUROG3<sup>LOW</sup> and NEUROG3<sup>HIGH</sup> cells but found no difference (Figure S5C). p120ctn isoform switching from the shorter isoform 3 (Cas2) to the longer isoform 1 (Cas1), generated by alternative translation start sites, has been associated with more motile cells and EMT (Liu et al., 2014). We used an antibody specific for isoform 1 (Wu et al., 1998) and found no difference compared to results obtained with the antibody that recognizes both isoforms (Figures S5A and S5B). However, western blot of pancreata (mesenchyme and epithelium) from p120ctn FULL KO (Pdx1-Cre, p120ctn fl/fl, R26R) embryos revealed that a 120 kDa band equivalent to isoform 1 was retained while a 100 kDa band equivalent to isoform 3 was much reduced (Figure S6D), demonstrating that it is mainly isoform 3 that is expressed in the pancreatic epithelium.

### p120ctn Loss in Endocrine Progenitors Enhances Delamination and Their Conversion into an Alpha Cell Fate

To test the functional role of p120ctn during endocrinogenesis we ablated *Ctnnd1* within NEUROG3+ endocrine progenitors (Neurog3-Cre, p120ctn fl/fl, R26R, see Figure 5G). The Neurog3-Cre driver (Gu et al., 2002) induced efficient recombina-

tion of *Ctnnd1* at E14.5 (Figure 5H). Loss of p120ctn from NEUROG3+ cells did not affect cell expansion or survival (Figures S4I and S4S) but led to increased displacement of KO cells toward the outside of the epithelium (Figure 5H). The delaminated p120ctn KO cells were NEUROG3 negative and INS or Glucagon (GCG) positive (Figure 5H and inserts in Figure 5K). There was a significantly increased proportion of NEUROG3<sup>HIGH</sup> cells (Figures 5J and S4L) but no difference in the total number of NEUROG3+ cells (Figures 5H, 5I, S4J, and S4K). Differentiation analysis showed a tendency toward increased GCG+ alpha and decreased INS+ beta cell differentiation at E14.5 (Figures 5K-5M, S4G, and S4H) and significantly increased alpha (1.7-fold) and decreased beta (1.6-fold) cell differentiation at E18.5 (Figures 5N-5P, S4Q, and S4R). Acinar differentiation was unchanged (Figures S4M-S4P).

These results show that accelerated delamination of p120ctn KO cells increases NEUROG3 expression in endocrine progenitor cells. This could be due to either acceleration of the NEUROG3 low-to-high transition or a prolonged NEUROG3<sup>HIGH</sup> phase. Ultimately, increased delamination of NEUROG3<sup>HIGH</sup> cells favors endocrine alpha cell fate over beta cell fate.

### Delamination of the Endocrine Cell Lineage Occurs after Maturation into Hormone-Producing Cells

The finding that premature delamination of endocrine progenitor cells favors alpha cell over beta cell differentiation suggests that the time an endocrine progenitor spends in the trunk epithelium determines its fate. This observation is in line with our previous finding that beta cell, but not alpha cell differentiation depends on apical polarity dynamics (Löff-Öhlin et al., 2017). However, the data are difficult to reconcile with the current paradigm that the endocrine lineage exit the trunk epithelium already at the NEUROG3+ stage (Shih et al., 2013).

To determine at which stage the endocrine lineage delaminates from the trunk epithelium we analyzed cell differentiation and 3D localization at E14.5. The overall distribution of NEUROG3+ cells differed slightly from the distribution of Pdx1-derived  $\beta$ gal+ epithelial cells, while the distribution of INS+ cells differed greatly (Figure 6A). When tested as individual localization categories, NEUROG3+ populations did not differ significantly from the Pdx1-derived populations. In contrast, significantly fewer beta cells were apically polarized (10%,  $p < 0.0001$ . Figure 6A, example in Figure 6B), and the majority

(G-P) Endocrine specific p120ctn ablation with Neurog3-Cre.

(G) Schematic of the experiment.

(H) Confocal images of  $\beta$ gal, p120ctn, and NEUROG3 in HET (Neurog3-Cre  $\times$  p120ctn fl/+) and HOM KO (Neurog3-Cre  $\times$  p120ctn fl/fl) E14.5 pancreatic ducts. Note the mass of  $\beta$ gal+, p120ctn-, NEUROG3- cells adjoining the epithelium. Scale bar, 10  $\mu$ m. Arrows:  $\beta$ gal+, NEUROG3+ cells.

(I) Quantification of NEUROG3+,  $\beta$ gal+/ $\beta$ gal+ cells. Mean  $\pm$  SEM. ns, not significant (two-tailed t test). p120ctn HET (n = 3 embryos) and HOM KO (n = 4) embryos.

(J) Frequency distribution of NEUROG3 intensities in p120ctn WT (n = 181  $\beta$ gal- NEUROG3+ cells/3 embryos), HET (n = 91  $\beta$ gal+ NEUROG3+ cells/3 embryos), and HOM KO (n = 83  $\beta$ gal+ NEUROG3+ cells/4 embryos) at E14.5. p Value was calculated by a Kruskal-Wallis test (KW). WT and HET distributions were not significantly different.

(K) Confocal tile scan images of  $\beta$ gal, p120ctn, and INS (left) or GCG (right) in HET and HOM KO E14.5 pancreas. Scale bar, 100  $\mu$ m. Inserts: Magnified regions containing INS+/GCG+ cells. Scale bar, 10  $\mu$ m.

(L and M) Quantification of E14.5 IF staining for INS (L) and GCG (M). Mean  $\pm$  SEM. ns, not significant (two-tailed t test). p120ctn HET (n = 3 embryos) and HOM KO (n = 4 embryos).

(N) Confocal images of  $\beta$ gal, p120ctn, and INS or GCG in HET and HOM KO E18.5 pancreas. Scale bar, 20  $\mu$ m.

(O and P) Quantification of E18.5 IF staining for INS (O) and GCG (P). Mean  $\pm$  SEM. \* $p < 0.05$  (two-tailed t test). p120ctn HET n = 6 (INS)/4 (GCG) embryos and HOM KO n = 3 embryos.

See also Figures S4 and S5.

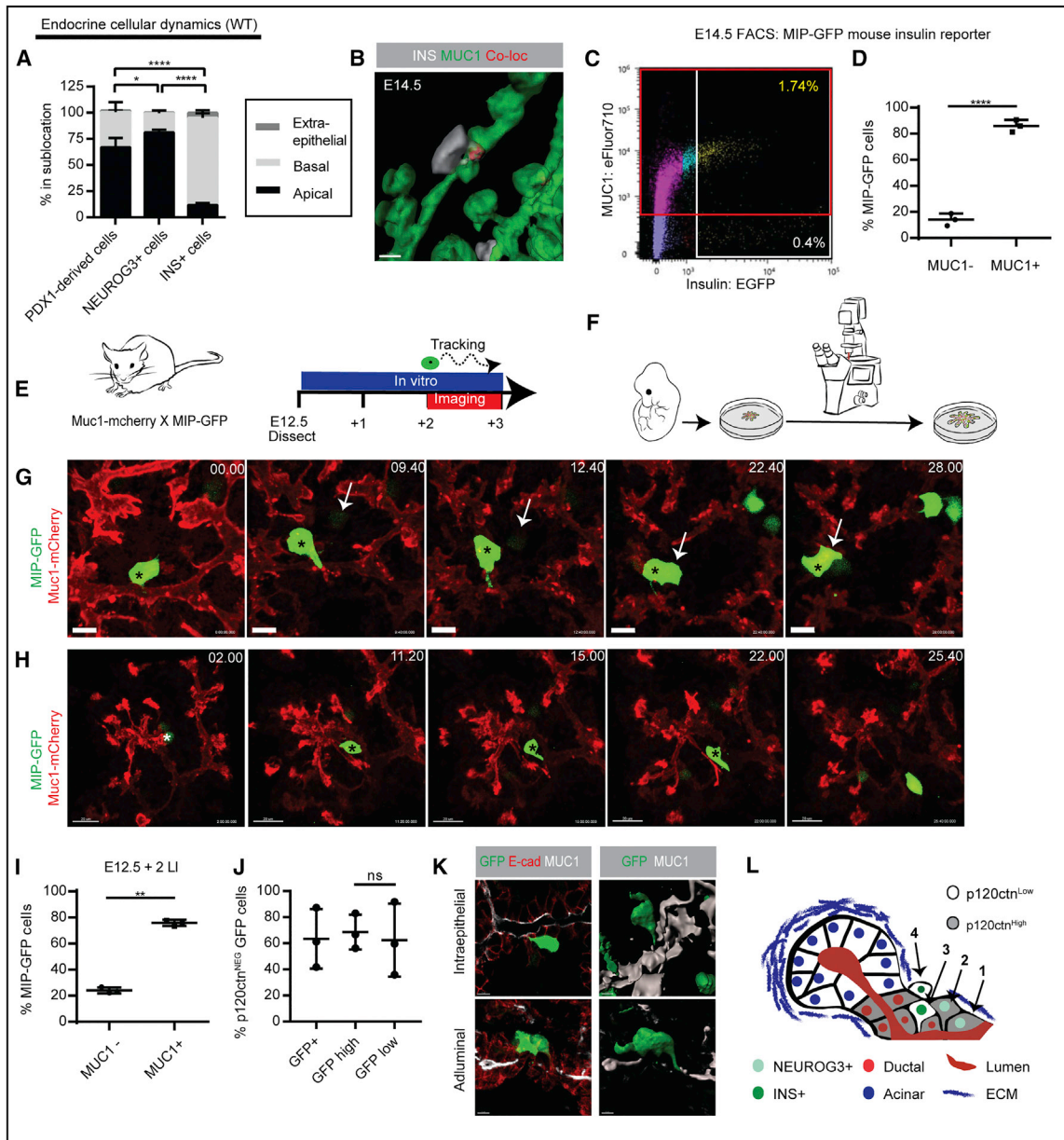


**Figure 6. Delamination of the Endocrine Cell Lineage Occurs after Maturation into Hormone-Producing Cells**

(A) Quantification of cell position in IF staining of either Pdx1-Cre lineage traced cells ( $\beta$ -gal+), NEUROG3+ cells or INS+ cells in thick sections of E14.5 pancreas. Cell position was determined based on MUC1, p120ctn/E-cad, and pan-Laminin staining. Mean  $\pm$  SD of  $n = 3$  WT embryos. p values for overall distributions were calculated using two-sided Fisher's exact test. \* $p < 0.05$ , \*\*\*\* $p < 0.0001$ . p values for each class calculated using multiple t test: Pdx1-derived versus NEUROG3+ cells  $p > 0.05$  for all classes; Pdx1-derived versus INS+  $p < 0.0001$  for both apical and basal fractions, but  $p > 0.5$  for the extraepithelial fraction.

(B) Surface rendering of whole-mount 3D IF staining of INS and MUC1 (based on Figure S5A) and their colocalization in E14.5 WT pancreas. Scale bar, 7  $\mu$ m.

(C) Example FACS plot of MUC1-eFluor710 versus INS-EGFP intensities in E14.5 pancreatic epithelial cells.

(D) Quantification of the fraction of MUC1<sup>-</sup> and MUC1<sup>+</sup> cells in the GFP<sup>+</sup> population. Mean  $\pm$  SEM of  $n = 3$  embryos. \*\*\*\* $p < 0.0001$  (two-tailed t test).

(E and F) Schematic of live imaging experiments with MIP-GFP insulin reporter and Muc1-mCherry apical polarity reporter.

(G and H) Maximum intensity projections of select regions from two different experiments.

(G) The GFP<sup>+</sup> cell (\*) retains a thin apical extension 0 to 22 h 40 min while clustering with another cell that appears at 9 h 40 min (arrow). Scale bar, 10  $\mu$ m.

(H) The GFP<sup>+</sup> cell (\*) is MUC1<sup>+</sup> when differentiating, and then slides along a newly formed lumen. Scale bar, 20  $\mu$ m.

(I) Quantification of MUC1 expression status at GFP-onset in the live imaging experiment. Mean  $\pm$  SEM of  $n = 3$  positions in 2 embryos. \*\* $p < 0.01$  (two-tailed t test).

(J) Quantification of p120ctn expression status in MIP-GFP<sup>+</sup> cells at E14.5. Mean  $\pm$  SEM of  $n = 3$  embryos. ns = not significant (two-tailed t test).

(K) IF staining of thick E14.5 MIP-GFP sections. Left: Confocal image of GFP, E-cad, and MUC1. Right: Surface rendering of GFP and MUC1.

(legend continued on next page)

of intra-epithelial beta cells were positioned with the cell body in the basal layer, without any contact with the lumen (83%,  $p < 0.0001$ ). This finding suggests that the endocrine lineage delaminates either at the very end of the NEUROG3+ stage or at the hormone-producing stage.

We have recently demonstrated by live imaging that NEUROG3+ cells move the cell body away from the epithelial lumen but retain an apical patch (Löf-Öhlin et al., 2017). For live imaging of INS+ cells, we crossed MIP-GFP *Insulin* reporter mice (Hara et al., 2003) with Mucin1-mCherry apical polarity reporter mice (Löf-Öhlin et al., 2017). Time-lapse imaging experiments starting at E12.5 + 2 days culture (developmentally equivalent to E13.5) were recorded for 38 h (Figures 6E and 6F). Tracking showed that 76% of GFP<sup>LOW</sup> cells are apically polarized (mCherry+) when they first appear (Figure 6I), and that loss of polarity in MIP-GFP cells occurs 2 to 3 h after the onset of GFP expression. Apical polarity is confined to a small domain on a thin membrane projection (Figure 6G; Videos S7A and S7B) similar to what is seen in NEUROG3<sup>HIGH</sup> cells. Notably, further maturation of beta cells—apparent by increased expression of GFP—is associated with formation of filopodia and lamellipodia, intraepithelial migration (Figure 6H; Video S7B), and clustering (Figure 6G; Video S7A) prior to delamination. 3D analysis of thick sections from E14.5 MIP-GFP embryos showed downregulation of p120ctn in the majority of GFP+ cells (Figure 6J) and confirmed that the majority of GFP+ cells were intraepithelial and that adluminal GFP+ cells (14%) have lost apical polarity (Figures 6K and S5F). FACS analysis of MIP-GFP cells from E14.5 pancreas stained for MUC1 confirmed these results as the majority of the GFP<sup>LOW</sup> cells still expressed MUC1, while GFP<sup>HIGH</sup> cells were mostly MUC1 negative (Figures 6C and 6D and controls in Figure S5E). We ascribe the discrepancy between the results from the FACS or live imaging and the immunofluorescence (IF) quantification to the increased sensitivity of the MIP-GFP transcriptional reporter and the caveat that thin apical projections can be easily missed in thick sections.

We conclude that beta cell differentiation is initiated prior to delamination and present a revised model for endocrine delamination (Figure 6L): p120ctn+ endocrine progenitors upregulate NEUROG3 expression as they move their cell bodies from a luminal (1 in Figure 6L) to a basal position (2) in the epithelium, while maintaining thin apically polarized projections. *Insulin* expression is gradually turned on as the committed endocrine progenitors downregulate p120ctn (3). Within a few hours, the new-born INS+ cells lose apical polarity and start migrating laterally within the epithelium to form clusters (not shown in model). The beta cell clusters remain attached to the basal side of the epithelium (4) but will eventually form the islets of Langerhans.

Altogether, our results strongly suggest that the time an endocrine progenitor spends in the trunk epithelium determines endocrine fate.

### E-Cadherin Acts Downstream of p120ctn

To explain how p120ctn KO cells can move within the epithelium, we analyzed their epithelial characteristics and apical polarity at E14.5 in 3D renderings of thick sections from the mosaic inducible p120ctn KO model (Pdx1-Cre-ER, p120ctn fl/fl, R26R induced at E8.5). Cells were scored as either luminal, stratified, or basal based on a MUC1, E-cad, and pan-Laminin staining. The overall distributions were significantly different between WT or HET and KO (Figures 7A and 7B). There was a significant loss of stratified p120ctn KO cells and an increase in basal and luminal KO cells. Apical polarity was significantly decreased, but cells with a normal size apical domain expressing CRB3 could still be observed (Figure 7C). The observed loss of cell stratification was mainly in p120ctn KO cells with WT neighbors. This cellular behavior could be due to relative surface tension changes: a WT-KO-WT cell triplet will minimize WT-KO interaction and maximize WT-WT interaction, which will result in rounding up and loss of stratification in KO cells.

In accordance with a relative change in surface tension, analysis of E14.5 mosaic inducible p120ctn KO embryos showed a dramatic downregulation of Cadherins and membrane-localized Beta-cat in all p120ctn KO cells (Figures 7D, 7E, and 7H). It was previously reported that ablation of p120ctn in the entire pancreatic epithelium did not affect E-cad expression (Hendley et al., 2015). However, repeating this analysis revealed a dramatic reduction in the expression of E-cad (Figures 7I and S6D). We found no changes in cortical actin (Figure S6A). Preservation of tight junction (TJ) was confirmed by ZO1, Claudin3, and Claudin7 (a rare member of the family that has baso-lateral as well as TJ association) antibody staining (Figures 7F, 7G, S6B, and S6C). TEM analysis of the p120ctn FULL KO at E18.5 also showed intact TJs (Figure 7J, red circles). However, the lateral membranes of neighboring KO cells exhibited several abnormalities, including reduced cell-cell contact (increased membrane distance) and interdigitating membranes in both ductal and acinar compartments (Figure 7J, arrows). This was especially clear when comparing to neighboring rare “WT” cells (Figure S6E). In conclusion, our analysis of junctional changes shows reduced lateral contact and cadherin expression, which is compatible with the hypothesis that mosaic p120ctn KO causes cell sorting due to differential surface tension.

We challenged this hypothesis by functionally testing whether mosaic loss of E-cad is sufficient to cause relocation of E-cad-deficient cells to the tip domain. *Cdh1* fl/fl (Boussadia et al., 2002) mice were crossed with Pdx1-Cre-ER and R26R mice to obtain Pdx1-Cre-ER, *Cdh1* fl/fl; R26R (mosaic E-cad KO) embryos. Tamoxifen was injected at E8.5 and the embryos were analyzed at E14.5 (Figure 7L). E-cad was lost in 16% of  $\beta$ gal+ cells (Figure S6G). Similar to the mosaic p120ctn KO model, E-cad KO cells were enriched in the peripheral CPA1+ tips (Figures 7M–7O). Manual counting of the number of tips with maximum one  $\beta$ gal-neg cell in a continuous tip epithelium (“green tips”, Figure 7P) revealed that this event was three-fold

(L) Drawing illustrating the proposed delamination mechanism. (1) A newly formed NEUROG3<sup>LOW</sup> cell with a large apical patch and high p120ctn expression. (2) The apical patch is reduced as the cell transitions to the NEUROG3<sup>HIGH</sup> stage. (3) *Insulin* expression is turned on and p120ctn down-regulated, but the cell remains in the epithelium. (4) After migrating inside the epithelium, and in some cases forming clusters with other INS+ cells (data not shown), the INS+, p120ctn<sup>LOW</sup> cell reduces the lateral domains, becomes depolarized, and attaches itself to the outside of the epithelium. See also Figure S5; Videos S7A and S7B.

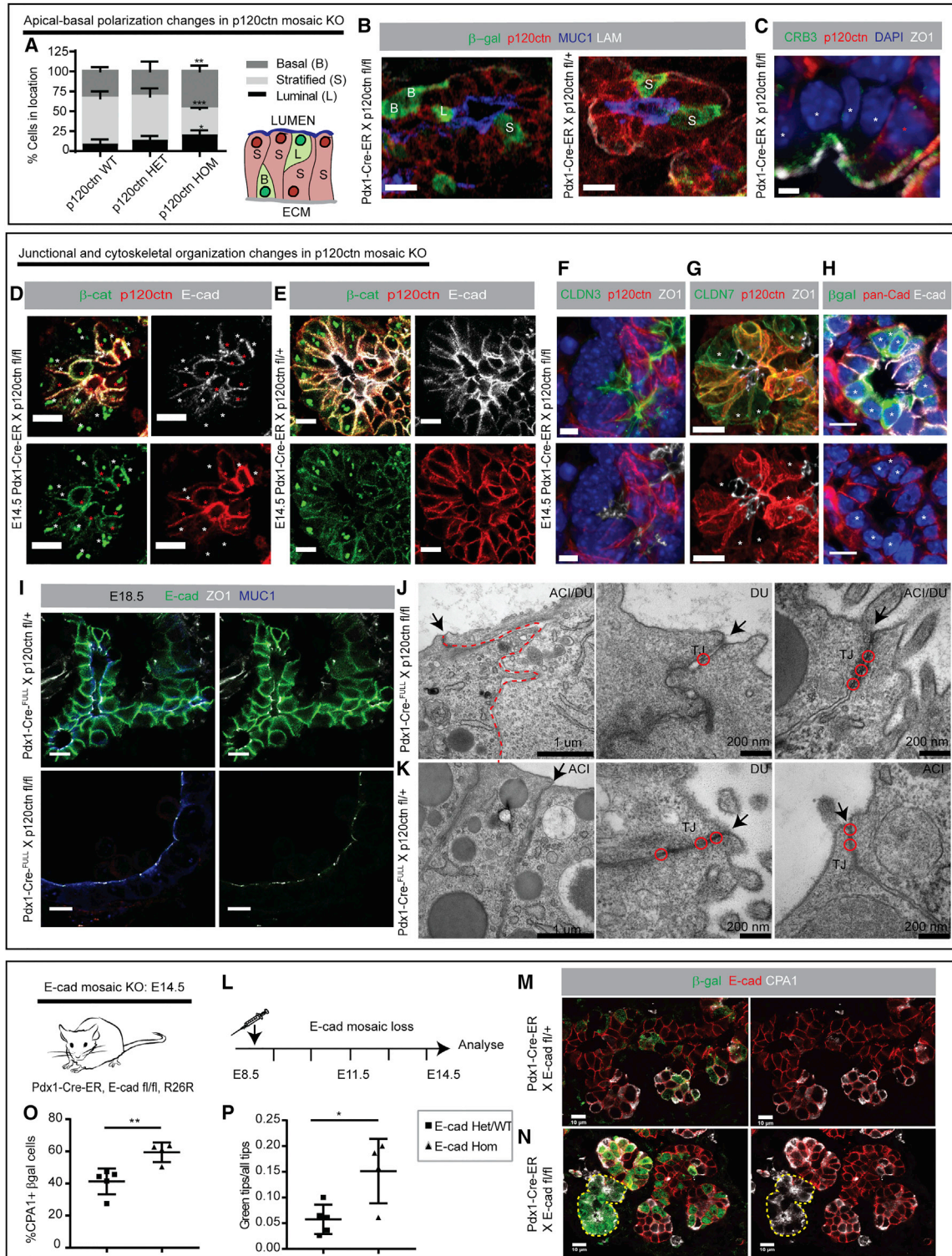


**Figure 7. E-Cadherin Acts Downstream of p120ctn**

(A–H) E14.5 Pdx1-Cre-ER × p120ctn fl/fl or fl/+ pancreas induced with tamoxifen from E8.5.

(A) Quantification of cell position based on 3D IF staining of MUC1, p120ctn, βgal, and pan-Laminin (LAM). Mean ± SEM of n = 3 E14.5 WT, n = 3 p120ctn HET, and n = 4 HOM KO embryos. \*p < 0.05, \*\*p < 0.01, \*\*\*p < 0.001 (multiple t test of each category comparing WT and HOM KO). The overall distribution (chi-square test) was significantly different between WT and HOM KO (p < 0.001) and HET and HOM KO (p < 0.01), but not between HET and WT (p > 0.9).

(B) Maximum intensity projection (MIP) of βgal, p120ctn, MUC1, and LAM in p120ctn HOM KO and HET pancreas. Scale bar, 10 μm.

(legend continued on next page)

more frequent in mosaic E-cad KO embryos (15%). This phenomenon was not due to an increase of  $\beta$ gal<sup>+</sup> cells in E-cad KO embryos (Figures S6F and S6I), and the total number of tips per epithelial area remained constant (Figure S6H).

In conclusion, mosaic ablation of E-cad leads to the same changes in organ patterning and differentiation as were observed by mosaic ablation of p120ctn lending support to E-cad being the major effector of p120ctn.

## DISCUSSION

The notion that organ architecture governs cellular fate has recently been challenged by findings that some progenitor clones are unipotent prior to organ patterning (Larsen et al., 2017; Sznurkowska et al., 2018), suggesting a predetermined fate. Our findings explain how these apparently contradictory models can be reconciled by demonstrating that individual cellular motility driven by p120ctn-mediated differential E-cad expression dictates localization to an instructive niche at the right time and place to guide cellular fate. This means that pancreatic progenitor clones with low p120ctn protein expression will appear to be acinar committed prior to patterning, when in fact they do not differ in their transcriptome compared to neighboring cells. We demonstrate that differential p120ctn driven motility dictates pancreatic progenitor fate indirectly by regulating both organ patterning and niche localization. We observed that p120ctn cells form isolated clusters at the periphery, where they function as branching initiator sites, which collectively migrate to form tips. Collective cell migration may also function during normal pancreatic morphogenesis, as a similar migration pattern and streaks of cells with low p120ctn expression is seen in WT embryos. It was recently proposed (Shih et al., 2016) that pancreatic progenitor cells downregulate AJ components in peripheral cap cells due to interaction with the ECM via integrin signaling. This, however, fails to explain why tip formation takes place at discrete sites. We propose a synthesis of the two models, where p120ctn<sup>LOW</sup> cells sort to discrete domains at the periphery, which are stabilized at the ECM interface by integrin signaling (McMillen and Holley, 2015). Differential surface tension models imply that cells will sort passively merely based on their differential surface tension. Although we cannot separate sorting from active migration with current *in vivo* techniques, our live-imaging experiments show

formation of filopodia and lamellipodia in polarized motile cells, indicating that active intraepithelial migration is occurring.

Differences in p120ctn expression not only set up the tip-niche at the periphery but also guide cells there. p120ctn ablation in pancreatic progenitors post-patterning is sufficient to drive re-localization and acinar differentiation. Future studies are needed in order to determine which physical characteristics of the tip-niche, as opposed to the trunk-niche, drives fate allocation. The ECM is a known acinar determinant (Crisera et al., 2000). Other possible determinants are curvature (tension), cell shape, proximity to mesenchyme (Li et al., 2004), and proximity to tubes.

Our results suggest that p120ctn regulates organ patterning through E-cad. p120ctn has also been shown to inactivate RHOA and activate CDC42 and RAC1 signaling. However, since *Cdc42* (Kesavan et al., 2009) and *Rac1* (Löf-Öhlin et al., 2017) ablation in the pancreas does not have tip-trunk patterning defects, we consider it unlikely that RAC1 and CDC42 act downstream of p120ctn in pancreatic patterning. E-cad and RHOA signaling are closely entwined (Marjoram et al., 2014), making it difficult to assess their independent roles. The fact that mosaic ablation of E-cad leads to the same changes in organ patterning and differentiation as p120ctn mosaic ablation strongly suggests that E-cad is the major downstream component of p120ctn.

p120ctn is used re-iteratively to regulate endocrine delamination from the trunk niche and balance alpha and beta cell specification. We propose a new model for this process, where beta cells are fully specified before they delaminate as a consequence of p120ctn downregulation. In a previous study, we showed that reduction of the apical domain is required for endocrine progenitors to commit to an endocrine fate (Löf-Öhlin et al., 2017). In our present study, we demonstrate that the next step of commitment to a specific endocrine fate also depends on apical polarization, as cells that are forced to downregulate p120ctn and delaminate through loss of apical polarity already at the NEUROG3<sup>+</sup> stage are biased toward an alpha cell fate. Previously, we showed that constitutive activation of CDC42 in newborn beta cells prevents delamination through failure to disassemble junctional actin (Kesavan et al., 2014). Therefore, reduced p120ctn may additionally trigger delamination via reduced CDC42 activity and disassembly of junctional actin.

Studying epithelial dynamics and differentiation has high clinical relevance since some of the most aggressive human cancers

(C–H) White\* = KO cell, red\* = WT cell.

(C) Confocal image of CRB3, p120ctn, ZO1, and DAPI in HOM KO. Scale bar, 3  $\mu$ m.

(D and E) Confocal image of Beta-cat, E-cad, and p120ctn in HOM KO (D) and HET (E) pancreas. Scale bar, 10  $\mu$ m.

(F) MIP of Claudin3 (CLDN3), ZO1, p120ctn, and DAPI showing preserved TJ's in HOM KO cells. Scale bar, 5  $\mu$ m.

(G) MIP of Claudin7 (CLDN7), ZO1, and p120ctn in HOM KO. Scale bar, 10  $\mu$ m.

(H) Confocal image of  $\beta$ gal, E-cad, Pan-Cadherin, and DAPI in HOM KO. Scale bar, 10  $\mu$ m.

(I–K) Analysis of E18.5 Pdx1-Cre-FULL  $\times$  p120ctn fl/fl or fl/+ pancreas.

(I) Confocal images of E-cad, ZO1, and MUC1. Scale bar, 10  $\mu$ m.

(J and K) TEM micrographs from FULL pancreatic HOM KO (J) and HET (K) E18.5 pancreas. Arrows: apical cell-cell junctions. Stippled line: cell-cell lateral border.

Circles: Tight junctions (TJ), ACI: acinar, DU: ductal. Scale bars, 1  $\mu$ m and 200 nm.

(L–P) Analysis of E14.5 Pdx1-Cre-ER  $\times$  E-cad fl/fl or fl/+ pancreas induced with tamoxifen from E8.5.

(L) Schematic of the experiment.

(M and N) Confocal images of  $\beta$ gal, E-cad, and CPA1 in HET (M) and HOM KO (N). Yellow stippled line outlines an E-cad<sup>-</sup> tip. Scale bar, 10  $\mu$ m.

(O and P) Quantification of IF staining. Mean  $\pm$  SEM of n = 5 E14.5 HET and n = 4 HOM KO embryos. \*p < 0.05, \*\*p < 0.01 (two-tailed t test).

(O) CPA1<sup>+</sup>,  $\beta$ gal<sup>+</sup> HET, and KO cells.

(P) Fraction of tips with  $\leq$  1  $\beta$ gal<sup>-</sup> cell in a continuous tip epithelium (“green tips”).

See also Figures S7 and S8.

originate from epithelia. When these cancer cells metastasize, they may subvert developmental programs allowing them to de-differentiate and spread. Downregulation of cell-cell adhesion molecules (CAMs), such as E-cad, is viewed as a required step in metastasis (Hanahan and Weinberg, 2000). Indeed, some therapeutic drugs target the upregulation of CAMs, especially E-cad (Wong et al., 2018). Our results, however, shed light on why p120ctn and E-cad have been found to function as both oncogenes and tumor suppressors depending on the tissue context (Peglion and Etienne-Manneville, 2013; Rodriguez et al., 2012). We show that it is the differential expression relative to neighboring normal cells, rather than the absolute level of the protein, which dictates its involvement in driving cell movement and delamination during development. The same could be true for regulation of metastasis. If so, this would mean that drugs targeting CAMs should be carefully titrated to normalize the expression of tumor cell CAMs to the levels of surrounding untransformed cells. Lastly, our finding that p120ctn is also downregulated during pancreatic endocrinogenesis in human fetal tissue means that targeting the p120ctn pathway could potentially help in the development of targeted alpha and beta cell protocols for differentiation of human embryonic stem cells.

## STAR★METHODS

Detailed methods are provided in the online version of this paper and include the following:

- **KEY RESOURCES TABLE**
- **CONTACT FOR REAGENT AND RESOURCE SHARING**
- **EXPERIMENTAL MODEL AND SUBJECT DETAILS**
  - In Vivo Mouse Studies
  - C57bl/6BomTac
  - E-cad-CFP, Pdx1-GFP
  - Ptf1a-Cre-ER, mTmG
  - Pdx1-Cre-ER, p120ctn fl/fl, R26R
  - Pdx1-Cre, p120ctn fl/fl, R26R or mTmG
  - Neurog3-Cre, p120ctn fl/fl, R26R
  - Muc1-mCherry, MIP-GFP
  - Neurog3-YFP
  - Pdx1-Cre-ER, Cdh1 fl/fl, R26R
  - Human Studies
  - Ex Vivo Mouse Studies
- **METHOD DETAILS**
  - Time-Lapse Imaging
  - Immunofluorescent Staining and Imaging
  - Transmission Electron Microscopy
  - Flow Cytometry and Cell Sorting
  - Immunoblotting
  - Quantitative PCR
  - Manual Image Processing and Quantification
  - Time-Lapse Imaging
  - Automated Image Analysis
  - Locating Cells in IF Images
  - Finding Final Nuclear Mask (Nuc\_mask) and Cellular Positions
  - Intensity Line Scans
  - Clustering Index
- **QUANTIFICATION AND STATISTICAL ANALYSIS**

## SUPPLEMENTAL INFORMATION

Supplemental Information can be found with this article online at <https://doi.org/10.1016/j.devcel.2019.02.005>.

## ACKNOWLEDGMENTS

We thank Ulf Tiemann for editing of the manuscript; Stella Felsch, Jelena Misokovic Krivokapic, Jette Larsen, and Diana Klüver Hansen for technical assistance; Raphael Scharfmann for supplying human fetal tissue; Rolf Kemler for the Cdh1 fl/fl mouse; and Christopher V. Wright for the Ptf1a-Cre-ER mouse. We acknowledge the Danstem Cytometry Core for FACS assistance and the Core Facility for Integrated Microscopy, Faculty of Health and Medical Sciences, University of Copenhagen for use of microscopes and assistance with TEM. This work was supported by JDRF grant 3-2011-214. The Novo Nordisk Foundation Center for Stem Cell Biology is supported by a Novo Nordisk Foundation grant number NNF17CC0027852.

## AUTHOR CONTRIBUTIONS

P.N. conceived the study; designed, conducted, and analyzed the experiments; and wrote the manuscript. S.H. developed the automated image analysis methods, created artwork, and edited the manuscript. Z.M.L.-Ö. conducted western blot and qPCR. N.F.P. conducted the 3D NEUROG3 cell position analysis. F.M.H. performed human fetal tissue staining. A.B.R. supplied the p120ctn fl/fl mouse and the Mab 6H11 antibody and edited the manuscript. H.S. conceived the study and wrote the manuscript.

## DECLARATION OF INTERESTS

The authors declare no competing interests.

Received: April 23, 2018

Revised: December 13, 2018

Accepted: February 4, 2019

Published: March 7, 2019

## REFERENCES

- Benjamini, Y., Krieger, A.M., and Yekutieli, D. (2006). Adaptive linear step-up procedures that control the false discovery rate. *Biometrika* 93, 491–507.
- Boussadia, O., Kutsch, S., Hierholzer, A., Delmas, V., and Kemler, R. (2002). E-cadherin is a survival factor for the lactating mouse mammary gland. *Mech. Dev.* 115, 53–62.
- Brodland, G.W. (2002). The differential interfacial tension hypothesis (DITH): A comprehensive theory for the self-rearrangement of embryonic cells and tissues. *J. Biomech. Eng* 124, 188–197.
- Cole, L., Anderson, M., Antin, P.B., and Limesand, S.W. (2009). One process for pancreatic beta-cell coalescence into islets involves an epithelial-mesenchymal transition. *J. Endocrinol* 203, 19–31.
- Crisera, C.A., Kadison, A.S., Breslow, G.D., Maldonado, T.S., Longaker, M.T., and Gittes, G.K. (2000). Expression and role of laminin-1 in mouse pancreatic organogenesis. *Diabetes* 49, 936–944.
- Davis, M.A., and Reynolds, A.B. (2006). Blocked acinar development, E-cadherin reduction, and intraepithelial neoplasia upon ablation of p120-catenin in the mouse salivary gland. *Dev. Cell* 10, 21–31.
- Ewald, A.J., Brenot, A., Duong, M., Chan, B.S., and Werb, Z. (2008). Collective epithelial migration and cell rearrangements drive mammary branching morphogenesis. *Dev. Cell* 14, 570–581.
- Foty, R.A., and Steinberg, M.S. (2005). The differential adhesion hypothesis: A direct evaluation. *Dev. Biol.* 278, 255–263.
- Gouzi, M., Kim, Y.H., Katsumoto, K., Johansson, K., and Grapin-Botton, A. (2011). Neurogenin3 initiates stepwise delamination of differentiating endocrine cells during pancreas development. *Dev. Dyn* 240, 589–604.
- Gu, G., Dubauskaite, J., and Melton, D.A. (2002). Direct evidence for the pancreatic lineage: NGN3+ cells are islet progenitors and are distinct from duct progenitors. *Development* 129, 2447–2457.

- Hamada, S., Satoh, K., Miura, S., Hirota, M., Kanno, A., Masamune, A., Kikuta, K., Kume, K., Unno, J., Egawa, S., et al. (2013). miR-197 induces epithelial-mesenchymal transition in pancreatic cancer cells by targeting p120 catenin. *J. Cell. Physiol* 228, 1255–1263.
- Hanahan, D., and Weinberg, R.A. (2000). The hallmarks of cancer. *Cell* 100, 57–70.
- Hara, M., Wang, X., Kawamura, T., Bindokas, V.P., Dizon, R.F., Alcoser, S.Y., Magnuson, M.A., and Bell, G.I. (2003). Transgenic mice with green fluorescent protein-labeled pancreatic  $\beta$ -cells. *Am. J. Physiol. Endocrinol. Metab.* 284, E177–E183.
- Haralick, R.M., and Shapiro, L.G. (1993). *Computer and Robot Vision* (Prentice Hall).
- Harris, A.K. (1976). Is cell sorting caused by differences in the work of intercellular adhesion? A critique of the steinberg hypothesis. *J. Theor. Biol.* 61, 267–285.
- Hendley, A.M., Provost, E., Bailey, J.M., Wang, Y.J., Cleveland, M.H., Blake, D., Bittman, R.W., Roeser, J.C., Maitra, A., Reynolds, A.B., et al. (2015). P120 catenin is required for normal tubulogenesis but not epithelial integrity in developing mouse pancreas. *Dev. Biol.* 399, 41–53.
- Hendley, A.M., Wang, Y.J., Polireddy, K., Alsina, J., Ahmed, I., Lafaro, K.J., Zhang, H., Roy, N., Savidge, S.G., Cao, Y., et al. (2016). P120 catenin suppresses basal epithelial cell extrusion in invasive pancreatic neoplasia. *Cancer Res.* 76, 3351–3363.
- Holland, A.M., Micallef, S.J., Li, X., Elefanty, A.G., and Stanley, E.G. (2006). A mouse carrying the green fluorescent protein gene targeted to the Pdx1 locus facilitates the study of pancreas development and function. *Genesis* 44, 304–307.
- Huang, L.-K., and Wang, M.-J.J. (1995). Image thresholding by minimizing the measures of fuzziness. *Pattern Recognit* 28, 41–51.
- Hutson, M.S., Brodland, G.W., Yang, J., and Viens, D. (2008). Cell sorting in three dimensions: topology, fluctuations, and fluidlike instabilities. *Phys. Rev. Lett.* 101, 148105.
- Ireton, R.C., Davis, M.A., van Hengel, J., Mariner, D.J., Barnes, K., Thoreson, M.A., Anastasiadis, P.Z., Matrisian, L., Bundy, L.M., Sealy, L., et al. (2002). A novel role for p120 catenin in E-cadherin function. *J. Cell Biol.* 159, 465–476.
- Jennings, R.E., Berry, A.A., Kirkwood-Wilson, R., Roberts, N.A., Hearn, T., Salisbury, R.J., Blaylock, J., Piper Hanley, K., and Hanley, N.A. (2013). Development of the human pancreas from foregut to endocrine commitment. *Diabetes* 62, 3514–3522.
- Kesavan, G., Sand, F.W., Greiner, T.U., Johansson, J.K., Kobberup, S., Wu, X., Brakebusch, C., and Semb, H. (2009). Cdc42-mediated Tubulogenesis controls cell specification. *Cell* 139, 791–801.
- Kesavan, G., Lieven, O., Mamidi, A., Öhlin, Z.L., Johansson, J.K., Li, W.C., Lommel, S., Greiner, T.U., and Semb, H. (2014). Cdc42/N-WASP signaling links actin dynamics to pancreatic  $\beta$  cell delamination and differentiation. *Development* 141, 685–696.
- Kuo, C.S., and Krasnow, M.A. (2015). Formation of a neurosensory organ by epithelial cell slithering. *Cell* 163, 394–405.
- Laird, D.J., von Andrian, U.H., and Wagers, A.J. (2008). Stem cell trafficking in tissue development, growth, and disease. *Cell* 132, 612–630.
- Lam, L., Lee, S.-W., and Suen, C.Y. (1992). Thinning methodologies—a comprehensive survey. *IEEE Trans. Pattern Anal. Machine Intell* 14, 869–885.
- Larsen, H.L., Martin-Coll, L., Nielsen, A.V., Wright, C.V.E., Trusina, A., Kim, Y.H., and Grapin-Botton, A. (2017). Stochastic priming and spatial cues orchestrate heterogeneous clonal contribution to mouse pancreas organogenesis. *Nat. Commun* 8, 605.
- Li, C.H., and Tam, P.K.S. (1998). An iterative algorithm for minimum cross entropy thresholding. *Pattern Recognit. Lett.* 19, 771–776.
- Li, Z., Manna, P., Kobayashi, H., Spilde, T., Bhatia, A., Preuett, B., Prasad, K., Hembree, M., and Gittes, G.K. (2004). Multifaceted pancreatic mesenchymal control of epithelial lineage selection. *Dev. Biol.* 269, 252–263.
- Liu, X., Yi, C., Wen, Y., Radhakrishnan, P., Tremayne, J.R., Dao, T., Johnson, K.R., and Hollingsworth, M.A. (2014). Interactions between MUC1 and p120 catenin regulate dynamic features of cell adhesion, motility, and metastasis. *Cancer Res.* 74, 1609–1620.
- Löf-Öhlin, Z.M., Nyeng, P., Bechard, M.E., Hess, K., Bankaitis, E., Greiner, T.U., Ameri, J., Wright, C.V., and Semb, H. (2017). EGFR signalling controls cellular fate and pancreatic organogenesis by regulating apicobasal polarity. *Nat. Cell Biol.* 19, 1313–1325.
- MacDonald, R.J., Swift, G.H., and Real, F.X. (2010). Transcriptional control of acinar development and homeostasis. *Prog. Mol. Biol. Transl. Sci.* 97, 1–40.
- Manning, M.L., Foty, R.A., Steinberg, M.S., and Schoetz, E.M. (2010). Coaction of intercellular adhesion and cortical tension specifies tissue surface tension. *Proc. Natl. Acad. Sci. USA* 107, 12517–12522.
- Marjoram, R.J., Lessey, E.C., and Burridge, K. (2014). Regulation of RhoA activity by adhesion molecules and mechanotransduction. *Curr. Mol. Med* 14, 199–208.
- McCrea, P.D., and Park, J.I. (2007). Developmental functions of the P120-catenin sub-family. *Biochim. Biophys. Acta* 1773, 17–33.
- McMillen, P., and Holley, S.A. (2015). Integration of cell-cell and cell-ECM adhesion in vertebrate morphogenesis. *Curr. Opin. Cell Biol.* 36, 48–53.
- Mellitzer, G., Martin, M., Sidhoum-Jenny, M., Orvain, C., Barths, J., Seymour, P.A., Sander, M., and Gradwohl, G. (2004). Pancreatic islet progenitor cells in neurogenin 3-yellow fluorescent protein knock-add-on mice. *Mol. Endocrinol* 18, 2765–2776.
- Muzumdar, M.D., Tasic, B., Miyamichi, K., Li, L., and Luo, L. (2007). A global double-fluorescent Cre reporter mouse. *Genesis* 45, 593–605.
- Noren, N.K., Liu, B.P., Burridge, K., and Kreft, B. (2000). p120 catenin regulates the actin cytoskeleton via Rho family GTPases. *J. Cell Biol.* 150, 567–580.
- Otsu, N. (1979). A threshold selection method from gray-level histograms. *IEEE Trans. Syst. Man Cybern* 9, 62–66.
- Pan, F.C., Bankaitis, E.D., Boyer, D., Xu, X., Van de Casteele, M., Magnuson, M.A., Heimberg, H., and Wright, C.V.E. (2013). Spatiotemporal patterns of multipotentiality in Ptf1a-expressing cells during pancreas organogenesis and injury-induced facultative restoration. *Development* 140, 751–764.
- Peglion, F., and Etienne-Manneville, S. (2013). P120Catenin alteration in cancer and its role in tumour invasion. *Philos. Trans. R. Soc. Lond. B. Biol. Sci.* 368, 20130015.
- Puri, S., and Hebrok, M. (2007). Dynamics of embryonic pancreas development using real-time imaging. *Dev. Biol.* 306, 82–93.
- Rodriguez, F.J., Lewis-Tuffin, L.J., and Anastasiadis, P.Z. (2012). E-cadherin's dark side: possible role in tumor progression. *Biochim. Biophys. Acta* 1826, 23–31.
- Rueden, C.T., Schindelin, J., Hiner, M.C., DeZonia, B.E., Walter, A.E., Arena, E.T., and Eliceiri, K.W. (2017). ImageJ2: ImageJ for the next generation of scientific image data. *BMC Bioinformatics* 18, 529.
- Rukstalis, J.M., and Habener, J.F. (2007). Snail2, a mediator of epithelial-mesenchymal transitions, expressed in progenitor cells of the developing endocrine pancreas. *Gene Expr. Patterns* 7, 471–479.
- Shakya, R., Watanabe, T., and Costantini, F. (2005). The role of GDNF/Ret signaling in ureteric bud cell fate and branching morphogenesis. *Dev. Cell* 8, 65–74.
- Shih, H.P., Wang, A., and Sander, M. (2013). Pancreas organogenesis: From lineage determination to morphogenesis. *Annu. Rev. Cell Dev. Biol.* 29, 81–105.
- Shih, H.P., Panlasigui, D., Cirulli, V., and Sander, M. (2016). ECM signaling regulates collective cellular dynamics to control pancreas branching morphogenesis. *Cell Rep* 14, 169–179.
- Snippert, H.J., van der Flier, L.G., Sato, T., van Es, J.H., van den Born, M., Kroon-Veenboer, C., Barker, N., Klein, A.M., van Rheenen, J., Simons, B.D., et al. (2010). Intestinal crypt homeostasis results from neutral competition between symmetrically dividing Lgr5 stem cells. *Cell* 143, 134–144.
- Soriano, P. (1999). Generalized lacZ expression with the ROSA26 Cre reporter strain. *Nat. Genet.* 21, 70–71.

- Sugiyama, T., Rodriguez, R.T., McLean, G.W., and Kim, S.K. (2007). Conserved markers of fetal pancreatic epithelium permit prospective isolation of islet progenitor cells by FACS. *Proc. Natl. Acad. Sci. USA* *104*, 175–180.
- Sznurkowska, M.K., Hannezo, E., Azzarelli, R., Rulands, S., Nestorowa, S., Hindley, C.J., Nichols, J., Göttgens, B., Huch, M., Philpott, A., et al. (2018). Defining lineage potential and fate behavior of precursors during pancreas development. *Dev. Cell* *46*, 360–375.e5.
- Villasenor, A., Chong, D.C., Henkemeyer, M., and Cleaver, O. (2010). Epithelial dynamics of pancreatic branching morphogenesis. *Development* *137*, 4295–4305.
- Vincent, L. (1993). Morphological grayscale reconstruction in image analysis: applications and efficient algorithms. *IEEE Trans. Image Process* *2*, 176–201.
- Wong, S.H.M., Fang, C.M., Chuah, L.H., Leong, C.O., and Ngai, S.C. (2018). E-cadherin: its dysregulation in carcinogenesis and clinical implications. *Crit. Rev. Oncol. Hematol* *121*, 11–22.
- Wu, J., Mariner, D.J., Thoreson, M.A., and Reynolds, A.B. (1998). Production and characterization of monoclonal antibodies to the catenin p120ctn. *Hybridoma* *17*, 175–183.
- Zhou, Q., Law, A.C., Rajagopal, J., Anderson, W.J., Gray, P.A., and Melton, D.A. (2007). A multipotent progenitor domain guides pancreatic organogenesis. *Dev. Cell* *13*, 103–114.

## STAR★METHODS

### KEY RESOURCES TABLE

REAGENT or RESOURCE	SOURCE	IDENTIFIER
<b>Antibodies</b>		
Rabbit polyclonal anti-Amylase (IHC 1:500)	Sigma-Aldrich	A8273
Rabbit polyclonal anti-Sox9 (IHC 1:1000)	Millipore	AB5535
Rabbit polyclonal anti-beta-galactosidase (IHC 1:2500)	MP Biomedicals	55976
Rabbit polyclonal anti-Neurogenin3 (IHC 1:2000)	Beta cell biology Consortium	AB2011
Rabbit polyclonal anti-Claudin3 (IHC 1:1000)	Invitrogen	34-1700
Rabbit polyclonal anti-Claudin7 (IHC 1:1000)	Nordic Biosite	E10590
Rabbit polyclonal anti-beta-catenin (IHC 1:2000)	Lifespan Biosciences	LS-C47531 No longer in production
Rabbit polyclonal anti-pan-laminin (IHC 1:750)	Sigma-Aldrich	L9393
Rabbit polyclonal anti-Zo1 (IHC 1:50)	Invitrogen	402200 RRID: AB_2533456
Rabbit polyclonal anti-Crb3 (IHC 1:20)	Novus Biologicals	NBP1-81185
Rabbit monoclonal anti-RhoA (clone 67B9) (IHC 1:100)	Cell Signaling Technology	2117
Rabbit monoclonal anti-alpha-tubulin (clone DM1A) (WB 1:1000)	Sigma	9026
Rabbit polyclonal anti-GATA4 (IHC 1:500)	Abcam	Ab84593 RRID:AB_10670538
Rabbit monoclonal anti MIST1/bHLHa15 (IHC 1:500)	Cell Signalling Technology	14896
Mouse polyclonal anti-p120ctn (pp120) (IHC and WB 1:400, FACS 1:1000)	BD Transduction Labs	610134
Mouse monoclonal anti-p120ctn isoform1 (Mab 6H11) (IHC 1:100)	Dr. A. Reynolds <a href="#">Wu et al. (1998)</a>	Mab 6H11
Mouse monoclonal anti-PAN-cadherin (clone CH19) (IHC 1:50)	Abcam	Ab6528
Mouse monoclonal anti-CD227 (Muc1) PE conjugated (clone16A) (FACS 1:100)	Biolegend	355603 RRID: AB_2561643
Goat polyclonal anti-CPA1 (IHC 1:100)	R and D systems	AF2765
Goat polyclonal anti-Pdx1 (IHC 1:1000)	Beta cell biology Consortium	2027
Rat monoclonal anti-E-cadherin (clone ECCD2) (IHC and WB 1:200)	Takara Bio	M108
Armenian Hamster polyclonal anti-Mucin1 (clone MH1, same as CT2) (IHC 1:500)	Thermo Scientific	HM-1630-P0
Guinea pig polyclonal anti-Insulin (IHC 1:750)	Linco/Agilent-DAKO	A056401-2
Guinea pig polyclonal anti-Glucagon (IHC 1:800)	Linco/Agilent-DAKO	4031-6H No longer in production
Guinea pig polyclonal anti-SOX9 (IHC 1:2000)	BCBC (kind gift of Ole Madsen)	
Alexa Fluor-488 Phalloidin (IHC 1:500)	Invitrogen	A12379
Rat monoclonal anti-CD133 (Prominin) APC conjugated (clone13A4) (FACS 1:100)	eBioscience/Invitrogen	17-1331-81 RRID: AB_823120
Rat polyclonal anti-CD49f PE conjugated (FACS 1:100)	BD biosciences	555763
Sheep polyclonal anti-NGN3 (IHC 1:400)	R&D	AF3444
<b>Biological Samples</b>		
Human fetal pancreas week 10.5 and 12.5	Raphael Scharfmann	
<b>Chemicals, Peptides, and Recombinant Proteins</b>		
Fibronectin bovine protein	Thermo-Fisher	33010018
Tamoxifen	Sigma-Aldrich	T5648

(Continued on next page)

**Continued**

REAGENT or RESOURCE	SOURCE	IDENTIFIER
Critical Commercial Assays		
TSA-Fluorescein kit	PerkinElmer	NEL701A001KT
Experimental Models: Organisms/Strains		
Mouse: C57BL/6BomTac	Taconic	B6JBOM-F/M
Mouse: Pdx1-GFP: Pdx1tm1Egs	<a href="#">Holland et al. (2006)</a>	RRID:MGI:3695580
Mouse: Ecad-CFP: Cdh1tm1Cle	<a href="#">Snippert et al., (2010)</a>	RRID:IMSR_JAX:016933
Mouse: Ptf1a-Cre-ER: Ptf1atm2(cre/ESR1)Cvw	<a href="#">Pan et al., (2013)</a>	RRID:BCBC_244
Mouse: mTmG: B6.129(Cg)-Gt(ROSA)26Sortm4 (ACTB-tdTomato,-EGFP)Luo/J	The Jackson Laboratory <a href="#">Muzumdar et al., (2007)</a>	007676; RRID:IMSR_JAX:007676
Mouse: Pdx1-Cre-ER: Tg(Pdx1-cre/Esr1*)35.10Dam	<a href="#">Gu et al., (2002)</a>	MGI:2684321
Mouse: p120ctn fl/+; Ctnnd1tm1Abre on C57BL/6 background	<a href="#">Davis and Reynolds, (2006)</a>	MGI:3617486
Mouse: R26R: B6.129S4-Gt(ROSA)26Sortm1Sor/J	The Jackson Laboratory <a href="#">Soriano, (1999)</a>	003474; RRID:IMSR_JAX:003474
Mouse: Pdx1-Cre: Tg(Pdx1-cre)89.1Dam	<a href="#">Gu et al., (2002)</a>	MGI:2684317
Mouse: Ngn3-Cre: Tg(Neurog3-cre)1Dam	<a href="#">Gu et al., (2002)</a>	MGI:4366451; RRID:IMSR_JAX:023973
Mouse: Muc1-mcherry 12M	<a href="#">Löf-Öhlin et al., 2017</a>	N/A
Mouse: Ngn3-YFP: Neurog3tm1Ggr	<a href="#">Mellitzer et al., 2004</a>	MGI:3505733
Mouse: Cdh1 fl/+; Cdh1tm2Kem	<a href="#">Boussadia et al., 2002</a>	MGI:2389020; RRID:IMSR_JAX:005319
Oligonucleotides		
Primer: Actb ( $\beta$ -actin) forward: TGTTACCAACTGG GACGACA	This paper	N/A
Primer: Actb ( $\beta$ -actin) reverse: GGGGTGTTGAAG GTCTCAA	This paper	N/A
Primer: Ctnnd1 forward: ATCTGAACTCAACGGACCC	This paper	N/A
Primer: Ctnnd1 reverse: GTCCCATCATCTGTGGTCTC	This paper	N/A
Primer: Muc1-mCherry genotyping forward: ATCGGG GTTTTACCTGGAAG	This paper	N/A
Primer: Muc1-mCherry genotyping reverse: ACCTTGAA GCGCATGAACTC	This paper	N/A
Software and Algorithms		
Fiji 2.0/ImageJ version 1.51u	<a href="#">Rueden et al., (2017)</a>	<a href="http://imagej.nih.gov/ij">http://imagej.nih.gov/ij</a>
Imaris version 8.4, 9.0	Bitplane	N/A
MATLAB R2016a version 9.0.0	MathWorks	N/A

**CONTACT FOR REAGENT AND RESOURCE SHARING**

Further information and requests for resources and reagents should be directed to and will be fulfilled by the Lead Contact, Henrik Semb ([semb@sund.ku.dk](mailto:semb@sund.ku.dk)). Request for the Muc1-mCherry mouse will be subject to an MTA.

**EXPERIMENTAL MODEL AND SUBJECT DETAILS**

**In Vivo Mouse Studies**

All mice were housed at the Department for Experimental Medicine at Copenhagen University as approved by “Miljø- og fødevarer- og fødevarerministeriet – Dyrforsøgstilsynet”. Male and female embryos at gestational age E11.5-E18.5 were used for experiments as indicated in the results section and below. Plugging males (12 weeks-2 years of age) were single housed, while females (8 weeks-20 weeks of age) were group housed. For time mating, 1-2 females were added to the male cage in the afternoon and vaginal plug was checked every morning for up to 3 days. The day of vaginal plug was recorded as E0.5. Littermates were used as controls in all experiments. Embryos were dissected at noon on the indicated day and tissue from one limb bud used for genotyping with the REDEExtract-N-Amp kit (Sigma-Aldrich) with the primers described in the papers cited for each mouse strain. Muc1-mCherry genotyping primers are listed in the [Key Resources Table](#).

### **C57bl/6BomTac**

C57bl/6BomTac (*Taconic*), hereafter designated C57bl/6, males were time mated with C57bl/6 females to obtain C57bl/6 (WT) embryos used in IF analysis involving only WT tissue.

### **E-cad-CFP, Pdx1-GFP**

Pdx1-GFP (Holland et al., 2006) heterozygous males (maintained on C57bl/6 background) were time mated with E-cad-CFP (Snippert et al., 2010) homozygous (maintained as a homozygous colony) females to obtain Pdx1-GFP heterozygous; E-cad-CFP heterozygous embryos at gestational age E11.5 and E14.5 for FACS studies.

### **Ptf1a-Cre-ER, mTmG**

Ptf1a-Cre-ER (Pan et al., 2013) heterozygous males (maintained on C57bl/6 background) were time mated with mTmG (Muzumdar et al., 2007) homozygous females (maintained as a homozygous colony) to obtain Ptf1a-Cre-ER heterozygous, mTmG heterozygous embryos at gestational age E11.5 for live imaging studies.

### **Pdx1-Cre-ER, p120ctn fl/fl, R26R**

Pdx1-Cre-ER (Gu et al., 2002) heterozygous (maintained on C57bl/6 background), *Ctnnd1*<sup>tm1Abre</sup> (Davis and Reynolds, 2006) hereafter named p120ctn fl/+ (maintained on C57bl/6 background), R26R (Soriano, 1999) homozygous males were time mated with p120ctn fl/+, R26R homozygous females to obtain Pdx1-Cre-ER heterozygous or WT; p120ctn +/+, fl/+ or fl/fl; R26R homozygous embryos at gestational age E11.5, E12.5, E14.5, E15.5 or E18.5 for IF studies. Tamoxifen dissolved in corn oil (1.5mg/animal) was injected intraperitoneally (i.p.) in pregnant females at E8.5, E11.5 or E12.5 to induce recombination. In Pdx1-Cre-ER, p120ctn fl/fl, R26R embryos, >80% of beta-galactosidase positive cells ( $\beta$ gal<sup>+</sup>) still expressed p120ctn protein six days after tamoxifen injection (Figure S2B), demonstrating less efficient recombination of the *Ctnnd1* locus compared to the *Rosa26* locus. Therefore, we selectively analyzed the p120ctn<sup>NEG</sup>;  $\beta$ gal<sup>+</sup> (designated  $\beta$ gal<sup>+</sup> in figures and legends) population by manual quantifications, while all  $\beta$ gal<sup>+</sup> cells were included in automated analysis.

### **Pdx1-Cre, p120ctn fl/fl, R26R or mTmG**

Pdx1-Cre (Gu et al., 2002) heterozygous (maintained on C57bl/6 background); p120ctn fl/+; R26R homozygous males were tested for recombination efficiency by time mating with mTmG homozygous females. Freshly isolated pancreata from E11.5 embryos were squashed between coverglass and object glass and analyzed directly under a widefield LEICA DM5500 microscope. Average recombination efficiency was assessed from green/red ratios in images from at least 4 Cre positive embryos and each male was assigned to Pdx1-Cre-LOW (20-30% efficiency in embryos), or Pdx1-Cre-FULL (80-100% efficiency in embryos) classes. Males giving rise to embryos with recombination ratios falling outside these categories were not used in the study.

Pdx1-Cre-LOW heterozygous, p120ctn fl/+; R26R homozygous males were time mated with p120ctn fl/fl; mTmG homozygous females to obtain Pdx1-Cre-LOW heterozygous or WT; p120ctn fl/+ or fl/fl; mTmG heterozygous; R26R heterozygous embryos at gestational age E12.5 for live imaging studies.

Pdx1-Cre-FULL heterozygous; p120ctn fl/+; R26R homozygous males were time mated with p120ctn fl/+; R26R homozygous females to obtain Pdx1-Cre-ER heterozygous or WT; p120ctn +/+, fl/+ or fl/fl; R26R homozygous embryos at gestational age E14.5 and E18.5 for IF studies.

### **Neurog3-Cre, p120ctn fl/fl, R26R**

Neurog3-Cre (Gu et al., 2002) heterozygous (maintained on C57bl/6 background); p120ctn fl/+; R26R homozygous males were time mated with p120ctn fl/+; R26R homozygous females to obtain Neurog3-Cre heterozygous or WT; p120ctn +/+, fl/+ or fl/fl; R26R homozygous embryos at gestational age E14.5 and E18.5 for IF studies.

### **Muc1-mCherry, MIP-GFP**

Muc1-mCherry 12M (Löff-Öhlin et al., 2017) (maintained on C57bl/6 background) heterozygous males/females were time mated to MIP-GFP (Hara et al., 2003) (maintained on C57bl/6 background) heterozygous females/males to obtain Muc1-mCherry 12M heterozygous; MIP-GFP heterozygous embryos at gestational age E12.5 for live imaging or E14.5 for sectioning and staining.

### **Neurog3-YFP**

Neurog3-YFP (Mellitzer et al., 2004) heterozygous males (maintained on C57bl/6 background) were time mated to C57bl/6 females to obtain Neurog3-YFP heterozygous embryos at gestational age E15.5 for cell sorting and RNA analysis.

### **Pdx1-Cre-ER, Cdh1 fl/fl, R26R**

Pdx1-Cre-ER, *Cdh1* fl/+ (Boussadia et al., 2002) (maintained on C57bl/6 background), R26R homozygous males were time mated with *Cdh1* fl/+, R26R homozygous females to obtain Pdx1-Cre-ER heterozygous or WT; *Cdh1* +/+, fl/+ or fl/fl; R26R homozygous embryos at gestational age E14.5 for IF studies. Tamoxifen dissolved in corn oil (1.5mg/animal) was injected intraperitoneally (i.p.) in pregnant females at E8.5 to induce recombination.

## Human Studies

Fixed pancreatic tissue (gender unknown) from one each of 10.5, 10.6, and 12.5 wpc (weeks post conception) human fetuses was supplied by Raphael Scharfmann, French Institute of Health and Medical Research, Paris, France. The use of human tissue was approved by “French Agence de Biomedecine” (accreditation # PFS08-011) and informed consent was obtained from all donors.

## Ex Vivo Mouse Studies

### Explant Studies

Pancreatic dorsal buds were dissected from E11.5 and E12.5 embryos in cold PBS under a stereoscope. They were immediately transferred to a 30 mm #1.5 glass bottom dish (Willco) fitted with two silicon inserts (Ibidi), coated with 100 $\mu$ g/ml bovine fibronectin (Gibco), and filled with sterile filtered explant medium (Media M-199, 10% Fetal Bovine Serum, 1% Penicillin/Streptomycin and 0.5% Fungizone). The explants were cultured at 37°C, 5% CO<sub>2</sub>. Explant medium was replaced the next morning after explants had attached, and replaced every other day thereafter. For imaging, the medium was replaced with sterile filtered imaging medium (Media M-199 without Phenol red, 10% Fetal Bovine Serum, 1% Penicillin/Streptomycin and 0.5% Fungizone).

## METHOD DETAILS

### Time-Lapse Imaging

#### *Ptf1a-Cre-ER, mTmG Imaging*

4-OHT (2 $\mu$ M) was added to dorsal pancreata 2 hours after explanting. Cells expressing Cre-recombinase became GFP+ 11 hours after 4-OHT addition. The next morning, the explanted dorsal pancreata were transferred to a 37°C preheated on-stage incubator with 5% CO<sub>2</sub> inside a preheated incubator surrounding a Leica SP8 confocal microscope. Imaging using a HC PL APO CS2 20x/0.75 IMM objective with glycerol immersion was commenced after 1 hour equilibration. Mark and find mode was used when more than one explant was imaged per experiment. A z-stack for each explant was acquired every 15 minutes for 45-48 hours with scanning speed 400 using a hybrid detector for mCherry and a PMT for GFP detection. The 8 bit images were acquired at 1024X1024 resolution. Average stack size was 30 $\mu$ m.

#### *Pdx1-Cre, p120ctn fl/fl, mTmG and Muc1-mcherry, MIP-GFP Imaging*

The explanted dorsal pancreata were transferred to a 37°C preheated on-stage incubator with 5% CO<sub>2</sub> inside a preheated XL multi S1 incubator surrounding a Zeiss LSM780 confocal microscope. Imaging using a C-Apochromat 40x/1.20 W Corr M27 objective was commenced after 1 hour equilibration. Multiposition scanning was used when more than one explant was imaged per experiment. A z-stack for each explant was acquired every 10 minutes for 24-48 hours with pixel dwell time of 3.15 using the 32PMT GaAsP detector. The 8 bit images were acquired at 1024X1024 resolution. Average stack size was between 25-30 $\mu$ m with voxel size 0.3X0.3X1.0 (x,y,z).

We confirmed that the MIP-GFP reporter only labels a negligible portion of the endocrine progenitors (5% Ngn3+/GFP+), by 3D image quantification of GFP, Ngn3 and INS expression (Figures S5G–S5I). Curiously, some endocrine GFP cells are INS negative, but positive for GCG (15%) or the pan-endocrine marker Chromogranin A (94%). These are likely originating from early polyhormonal cells. Since we analyse cells that turn on GFP expression at the secondary transition (E12.5 +2 days culture), this is not likely to affect our time-lapse results.

### Immunofluorescent Staining and Imaging

Mouse embryonic stomach, pancreas, duodenum and spleen were dissected at the appropriate age and fixed in 4% paraformaldehyde (PFA) for 1 hour (h)-overnight (o.n.) depending on the size. For sections, the tissue was transferred to 30% sucrose 3h-o.n., 1:1 sucrose/OCT 1 h, 100% OCT 1h and frozen in OCT on dry ice. The tissue was sectioned at 6  $\mu$ m or 16  $\mu$ m using a Leica cryostat and mounted on Superfrost PLUS glass slides (Thermo Scientific). Human tissue sections were deparaffinized for 15 min in Xylene and rehydrated in descending alcohol series prior to staining.

For immunofluorescent staining (IF) a minimum of 3 mouse embryos per genotype or 1 human embryo per gestational age were stained. Sections were dried for 20 minutes (min) at 37°C, then washed in PBS. For staining of all human tissue and for mouse tissue with primary antibodies anti-NEUROG3, RhoA, Claudin3 and 7, Zo1, Pdx1 or Crb3, antigen retrieval was performed by boiling in 0.01M citrate buffer pH6 for 10 min, followed by 30 min cooling and washing. Sections were blocked for 1-3 hs using TSA blocking solution (PerkinElmer). Primary antibodies (see [Key Resources Table](#)) were applied o.n. at room temperature. Secondary antibodies (Alexa or Dylight conjugated antibodies from Invitrogen/Jackson ImmunoResearch and Cy3-conjugated IgG FcY1 specific antibody from Jackson ImmunoResearch) were applied at 1:500 or 1:1000 dilution for 1h after several PBS washes. For RhoA, NEUROG3 and MIST1 staining, 30 min 3% hydrogen peroxide incubation and TSA amplification (PerkinElmer) was performed according to manufacturer's instructions. Slides were subsequently washed in PBS and mounted with fluorescent mounting medium (DAKO) using #1.5 coverglasses. For IF staining of intact pancreatic buds (whole-mount, WM) the PFA fixed tissue was transferred to MeOH for 1h on ice and stored at -20C. Tissue was incubated in Dent's bleach for at least 2hs, followed by equilibration to PBST (1xPBS with 0.01% Tween) through a series of descending MeOH concentrations. The tissue was blocked in TSA-blocking buffer for minimum 2hs, washed repeatedly in PBST and incubated in primary antibody o.n. at 4C. The next day, the tissue was washed repeatedly in

PBST and incubated in secondary antibody o.n. at 4°C. On the 3rd day, the tissue was washed repeatedly in PBST and transferred to MeOH. Before imaging, the tissue was washed and mounted in BABB (1:2 benzyl-alcohol and benzyl-benzoate) in a glass depression slide.

Confocal imaging was performed on a Zeiss LSM780 confocal microscope equipped with a 32PMT GaAsP detector and two PMT's. Objectives used include: Plan Apochromat 20x/0.8 M27, Plan-Apochromat 40x/1.30 Oil DIC M27, and Plan-Apochromat 63x/1.40 Oil DIC M27. The 12 bit images were acquired at 1024X1024 resolution. Tiled images of entire pancreatic sections for manual and automated quantification were acquired using the 40x objective and Zen software tiling module. They were stitched using Zen module stitching. High resolution confocal imaging was performed on a Zeiss LSM880 confocal microscope using an Airyscanner in super resolution mode and a C Plan-Apochromat 40x/1.3 Oil objective. The 12 bit images were acquired at 1024X1024 resolution or higher.

### Transmission Electron Microscopy

Stomach, pancreas, duodenum and spleen from Pdx1-Cre, 3 p120ctn fl/fl and 3 p120ctn fl/+ littermates were dissected at E18.5 and fixed in 2% v/v glutaraldehyde in 0.05 M sodium phosphate buffer (pH 7.2). The tissues were prepared for transmission electron microscopy by the Core Facility for Integrated Microscopy at University of Copenhagen. Following isolation of suitable specimen blocks, the samples were rinsed three times in 0.15 M sodium phosphate buffer (pH 7.2) and subsequently postfixed in 1% w/v OsO<sub>4</sub> in 0.12 M sodium phosphate buffer (pH 7.2) for 2 h. The specimens were dehydrated in graded series of ethanol, transferred to propylene oxide and embedded in Epon according to standard procedures. Sections, approximately 60 nm thick, were cut with a Ultracut 7 (Leica, Vienna, Austria) and collected on copper grids with Formvar supporting membranes, stained with uranyl acetate and lead citrate, and subsequently examined with a Philips CM 100 Transmission electron microscope (Philips, Eindhoven, The Netherlands), operated at an accelerating voltage of 80 kV and equipped with an OSIS Veleta digital slow scan 2k x 2k CCD camera. Digital images were recorded with the ITEM software package.

### Flow Cytometry and Cell Sorting

#### *E-cad-CFP X Pdx1-GFP*

For cell sorting from E-cad-CFP X Pdx1-GFP embryos the pancreas was isolated at E11.5 or E14.5. GFP+ samples were identified in a stereoscope. One pancreas was analyzed per sample. Because of the small sample size, each sample was spiked with tissue from 1 (E14.5) or 8 (E11.5) limb buds. Samples were dissociated by incubation in 117U/mL Liberase TL (Roche) and DNase (1U/μl) at 37°C and 950 rpm for 20 min in a thermomixer. During incubation, samples were triturated every 3-4 min. After centrifugation, samples were washed in PBS/FBS and resuspended in 0.125% Trypsin-EDTA and DNase and incubated at 37°C and 950 rpm for 10 min. Trypsin was inactivated by centrifugation and resuspension in 10% FBS in DMEM, and samples were washed in PBS, filtered and stained with Ghost dye (Tonbo -780 conjugated). In order to exclude differentiated endocrine cells (Sugiyama et al., 2007) samples were stained with anti-CD133 APC conjugated antibody (1:100) for 30 min at 4°C. Samples were then washed in PBS/FBS and fixed in 2% PFA at room temperature (RT) for 15 min. After washing, mouse anti-p120ctn antibody (pp120, 1:1000) was applied for 30 min at 4°C. After washing, secondary antibody Cy3-a-mouse IgG FcY1 (Jackson ImmunoResearch) was applied for 10 min. Samples were washed and resuspended in PBS/FBS and immediately analyzed using a BD FACS Aria III sorter (BD Biosciences) equipped with 445nm/488nm, 375nm/405nm, 561nm, 633nm laser lines. Gating was determined based on the GFP-negative, unstained, and 2. antibody controls and the same gating was used for all samples in each experiment. The expression of the membrane protein CD133 was homogenous in the gated population (results not shown).

#### *MIP-GFP*

For cell sorting from MIP-GFP timed matings the pancreas was isolated at E14.5. Samples were dissociated and filtered following the method described above. Anti-CD227 (MUC1) PE conjugated antibody (1:100) was applied for 30 min at RT. After washing, DAPI was added to the resuspended cells as a viability marker. The cells were analyzed on a SH800 sorter (SONY) equipped with 488nm/638nm/405nm/561nm laser lines. Gating was determined based on the negative and unstained controls and the same gating was used for all samples in each experiment.

#### *Neurog3-YFP*

For cell sorting from Neurog3-YFP embryos, the pancreas was isolated at E15.5. Samples were dissociated and filtered following the method described above. In order to exclude differentiated endocrine cells samples were stained with anti-CD133 APC conjugated antibody (1:100) and anti-CD49f PE conjugated CD49f (1:100) which was applied for 30 min at 4°C. After washing, DAPI was added to the resuspended cells as a viability marker. The cells were sorted into YFP<sup>High</sup> (NEUROG3<sup>High</sup>) or YFP<sup>Low</sup> (NEUROG3<sup>Low</sup>) on a SH800 sorter (SONY) equipped with 488nm/638nm/405nm/561nm laser lines. Gating was determined based on the negative and unstained controls and the same gating was used for all samples in each experiment.

### Immunoblotting

Embryonic pancreata were lysed in RIPA buffer containing 1x phosphatase inhibitor cocktail (Sigma) and 1x pierce protease inhibitor (Thermo Scientific). The samples were boiled in Loading buffer (Novex) containing 80mM DTT and separated on a SDS-PAGE gel (Novex) before being transferred onto a nitrocellulose filter (GE Healthcare). The filter was blocked for 2hs in 5% milk and blotted

with primary antibodies overnight at 4°C in blocking solution. The blot was incubated with HRP-conjugated secondary antibodies for 1h and proteins were visualized by chemiluminescence (GE Healthcare). Alpha-Tubulin was used as loading control. Antibodies used are listed in the [Key Resources Table](#).

### Quantitative PCR

Total RNA was extracted using RNeasy Microkit (Qiagen), checked for quantity and quality on a Nanodrop spectrophotometer (Thermo Scientific), and reverse transcribed using Superscript III first strand synthesis kit (Invitrogen). Q-PCR was performed using the StepOnePlus™ system (Applied Biosystems) and SYBR Green Master Mix (Invitrogen). Each sample was run two times and the mean CT value was normalized to Actb ( $\beta$ -actin) expression as  $1.9^{(CT^{Actb}-CT^{tnd1})}$ . Relative gene expression was calculated by setting NEUROG3-High sample 1 expression to 1. Primer sequences are listed in the [Key Resources Table](#).

### Manual Image Processing and Quantification

#### 2D Images

Manual image processing and quantification of 2D images were performed in Fiji/ImageJ ([Rueden et al., 2017](#)). For manual quantification of specific cell types, randomized files containing stitched images of at least 3 entire 6  $\mu$ m pancreatic sections from at least 3 embryos per genotype were counted using the cell counter plugin. First, all beta-galactosidase cells were marked (without viewing other channels), then p120ctn- cells, and finally the specific cell types. Areas were measured in thresholded images. The optimal thresholding method for each staining was determined using the Try all option: Fiji2 default thresholding for SOX9, DAPI and INS (bright, high contrast staining), Li thresholding ([Li and Tam, 1998](#)) for AMY (grainy, cytosolic staining), Huang thresholding ([Huang and Wang, 1995](#)) for E-cadherin and p120ctn (membrane staining), and Otsu thresholding ([Otsu, 1979](#)) for CPA1 and beta-galactosidase (fuzzy, cytosolic staining). Examples of intensity profiles for p120ctn, CPA1 and SOX9 in [Figure S1C](#) and p120ctn, OCT4, MIST1 and SOX9 in [Figure S7J](#) were generated in Fiji by manually plotting the line from tip to trunk using the tip-trunk markers as guides. For manual quantification of “green tips”, tip structures with no more than one beta-galactosidase- cell in the tip were counted, as was the total number of tips. E-cadherin area was measured as described above.

#### 3D Images

Maximum intensity projection (MIP) rendering, iso-surface rendering, and quantification of 3D images were performed in Imaris. For manual quantification of cell position in 16  $\mu$ m sections, stitched tile scans of z-stacks covering an entire section were examined. The analysis in [Figures 5E, 5F, and S5D](#) included at least 3 sections from each of 3 WT embryos. For the analysis in [Figure 6A](#), at least two 16 $\mu$ m sections from each of 3 KO, 3 Het and 3 WT embryos were scored. The position of  $\beta$ -gal+, INS+ or NEUROG3+ cells in the E-cad/p120ctn stained epithelium relative to MUC1+ lumen and LAM+ basal membrane was determined in 3D mode by examining each cell from all angles.

### Time-Lapse Imaging

All movies and stills from time-lapse experiments using the mTmG mouse strain were generated in Imaris after normalization by median filtering. The Muc1-mCherry, MIP-GFP and Pdx1-Cre, p120ctn fl/fl, mTmG time-lapse datasets were corrected in x-y for drift and organ growth using automated Imaris translational drift correction based on the segmented GFP signal. Tracking of cells in the Ptf1a-Cre-ER, mTmG ([Figures 1A–1D](#)) and Muc1-mCherry, MIP-GFP experiments ([Figures 6G–6I](#)) was performed using the automated spot finding and tracking feature in Imaris, followed by extensive manual correction of spots and tracks. Cell division and apoptosis events was tracked manually based on cellular morphology and membrane dynamics. MUC1-expression in GFP+ cells was scored by evaluating raw signal and 3D volume renderings.

Analysis of the Muc1-mCherry, MIP-GFP datasets for GFP+ cell tracks showed comparable results to a previous publication ([Puri and Hebrok, 2007](#)). Out of 56 tracks, there were 50 clustering events. This number was however boosted due to repeated “cell kissing” events, where cells clustered, left, and re-clustered, and the total number of tracks with clustering during the recording was 13 (23%). The total distance traveled during the 38 hour recording by each cell/cluster (median=61 $\mu$ m) exceeded the displacement of the cell (median=23 $\mu$ m). The median speed recorded was 0.14  $\mu$ m/min.

The Muc1-mCherry fusion reporter produces bright spots inside cell bodies (hereafter called spots) located away from the apical membrane. The images were processed for video and image representation in MATLAB to remove small and bright spots such that the dimmer fluorescently labeled lumen surface remains: Original 4D (3 spatial dimensions and time) data where first 3D Gaussian filtered (std=0.5), and then 3D Median filtered with a 3x3x3 kernel in order to reduce noise. We call the processed result IM. In order to remove fluorescence that does not come from the lumen surface we produce different BW masks, which allows us to construct a final **Remove\_mask** which tells us which pixels to replace with background level intensity in order to remove unwanted spots. **Mask1**: We take the 99-percentile brightness threshold of **IM**. (I.e. this mask locates the very brightest objects – including some spots and also lumen tips which are often brighter than central lumens). **Mask2**: We take the 97-percentile threshold of **IM** and remove connected region less than 3000 voxels. (I.e. this mask locates medium brightest objects which are also reasonably large, meaning large connected lumens). **Mask3**: We take the 95-percentile threshold of **IM**. (I.e. this mask locates all bright objects). **Mask4**: We take **Mask3** and remove connected regions less than 3000 voxels. We then dilate the remaining structure with a sphere-shaped structuring element of radius 1 pixel. (I.e. this mask locates all bright large objects, meaning large connected lumens plus a bit of their immediate neighborhood).

### Remove\_Mask

this mask is equal to *Mask1* except objects which are also in *Mask2*. Joined with *Mask3* except objects which are also in *Mask4*. Finally **Remove\_mask** is dilated with a sphere-shaped structuring element of radius 1 pixel. We finally remove spots from **IM** by replacing voxels inside **Remove\_mask** with the corresponding voxels from a 3D median filtered original image (kernel 15x15x3).

### Automated Image Analysis

All automated image analysis was performed in MATLAB.

#### Tip Score

We have developed a method to access whether a particular cell is located in the tip domain or in the trunk domain based solely on the shape of the outline of the epithelium (Figures S7A–S7E), (see next section for explanation of the mask **mask\_epi**). Each point inside the epithelium outline receives a numeric score which is high when the point lies inside a tip area and low inside a trunk area.

Tip score at the point  $P = [x, y]$  inside the epithelial shape is defined as:

$$\text{Tip score}(x, y) = D_{MB}(x, y) - D_{SB}(x, y) - \sqrt{D_{CH}(x, y)} \quad (\text{Formula 1})$$

Where  $D_{MB}$  is the distance from  $P$  to the nearest mid-branch point (Figure S7C),  $D_{SB}$  is the distance from  $P$  to the nearest side-branch point (Figure S7D) and  $D_{CH}$  is the distance from  $P$  to the nearest convex hull point (Figure S7B). The reason that we use  $\sqrt{D_{CH}}$  and not  $D_{CH}$  in Formula (1) is that we do not want large values of  $D_{CH}$  at points in the trunk to dominate the expression too much. Note that if the tip score is calculated using lengths in pixels, it will depend on the resolution level. For our resolution level (pixel width/height equal to 0.2076mm), when we measure distance in units of pixel length, the tip score tends to fall in the range [-300;300].

**Skeletonization of the epithelial shape:** First, the binary image with the hand-drawn epithelial outline mask was median filtered (the median filtering returns another binary image) with a [3 3] kernel in order to remove small irregularities that would cause spurs. We then found the skeleton of the epithelial shape using first the iterative thinning algorithm described in (Haralick and Shapiro, 1993) and then the thinning algorithm described in (Lam et al., 1992). In some cases, we found that these algorithms stopped at a structure that still had a region more than a pixel wide left. In these cases, we alternated between the two algorithms until only a one-pixel-thick structure was left. We then removed all side branches of length <50 pixels in order to get rid of side branches that were there due to small bumps and not due to proper tip structures. We determined the location of all endpoints and all branching points in the skeleton structure.

The convex hull is defined as the smallest convex shape which encapsulates the epithelial outline (Figure S7B) and was determined using the `regionprops()` function of the image processing toolbox in MATLAB. We define mid branches as the pixels which are left if you keep only pixels NOT visited when starting at an endpoint and going one pixel at a time inward along the skeleton structure until either meeting a branching or having been through 200 pixels (Figure S7C).

We define side branches as the pixels in the skeleton structure, which are left if one keeps only pixels visited when starting at an endpoint and going one pixel at a time inward along the skeleton structure until either meeting a branching point or having been through 300 pixels (Figure S7D).

We validated our tip score by checking that cells/cell-pairs expressing known tip/trunk markers (CPA1 and SOX9) have a significantly higher and lower tip score respectively (Figures S7F–S7I). For CPA1 staining, the signal was in the cytosol (Figure S7F) and we were thus only able to assess via thresholding whether cells were positive or negative. For SOX9, the signal was in the nucleus (Figure S7F) and we could quantify expression level per cell. This was done by taking the median of the pixel values of the SOX9 channel inside one cell nucleus mask. The cell nuclear masks were generated using the DAPI channel (see section below where the generation of **Nuc\_mask** is explained). (The range of SOX9 intensities in different images were very similar and we did not need to normalize SOX9 intensities per image).

### Locating Cells in IF Images

#### For Determining a Nuclear Mask and Cell Positions (Cell Coordinates), We Make Use of Three Masks

**Hand drawn epithelial outline mask (mask\_epi):** We hand-drew the outline of the epithelial tissue for each image using a custom written MATLAB GUI. We will refer to this black and white (BW) mask as **mask\_epi**.

**Preliminary nuclear masks (I\_nuc\_otsu\_BW):** We first produce an enhanced image of cell nuclei from the DAPI channel, where we emphasize gaps between nuclei by subtracting the membrane/p120 signal from the DAPI signal, and call the result  $I_{nuc}$ . Then we reduce noise in  $I_{nuc}$  by Gaussian filtering,  $\text{std}=0.5$ . From  $I_{nuc}$  we produce a BW mask of nuclei  $I_{nuc\_otsu\_BW}$  by thresholding using Otsu's method (Otsu, 1979). Lastly, we fill holes and remove connected objects smaller than 80 pixels and set all pixels outside **mask\_epi** to zero/black to get the final **I\_nuc\_otsu\_BW**.

**Skeletonized membrane mask (skel\_mem\_BW):** First, we produce another enhanced (BW) mask of nuclei,  $I_{nuc\_med\_BW}$  which is used to clean up the membrane mask. This is done by first median filtering  $I_{nuc}$  with a kernel of size [15 15], producing  $I_{nuc\_med}$ . Then we make  $I_{nuc\_med\_BW}$  by letting all pixels in  $I_{nuc}$  greater than  $I_{nuc\_med}$  be one/white. We then set all pixels outside **mask\_epi** to zero/black, fill in holes and remove connected white region of size less than 200 pixels.

We produce a skeletonized membrane BW image, **skel\_mem\_BW**. This is done by first median filtering the membrane/p120 channel image  $C2$  with a kernel of size [15 15], producing  $skel\_mem\_med$ . Then we make **skel\_mem\_BW** by letting all pixels in  $C2$  greater

than *skel\_mem\_med* be one/white. We then set all pixels outside *mask\_epi* and *I\_nuc\_med\_BW* to zero/black, and run an iterative thinning algorithm described in (Haralick and Shapiro, 1993) to get the skeleton of the membrane mask.

### Finding Final Nuclear Mask (Nuc\_mask) and Cellular Positions

We erode the grayscale image *I\_nuc* with a disk-shaped structuring element of radius 4 producing *I\_nuc\_er*. We then perform morphological reconstruction by dilation (Vincent, 1993) using *I\_nuc\_er* as marker and *I\_nuc* as mask producing *I\_nuc\_MR*.

*I\_nuc\_MR* is then dilated with a disk-shaped structuring element of radius 20 and we use the negative of result *I\_nuc\_MR\_di* as mask for morphological reconstruction by dilation (Vincent, 1993) of the negative of *I\_nuc\_MR* (marker) producing the result *I\_nuc\_MR\_MR*.

We take the negative of *I\_nuc\_MR\_MR* and set pixels which are equal to one in *mask\_epi*, *skel\_mem\_BW* and in *I\_nuc\_otsu\_BW* equal to zero. The result *I\_nuc\_MR\_MR\_mask* can now be used to find the regional max marking the cell nuclei. Because some nuclei have several regional maxima close together we do morphological closing with a disk-shaped structuring element of radius 1 in order to merge these regions. Further, we assess that regional max regions smaller than 20 pixels are mostly due to noise and not cell nuclei so we remove these. The resulting **Nuc\_mask** is used as the final nuclear mask, and the centers of masses of the regions in **Nuc\_mask** are used as the position of cells in the epithelium (for an example see yellow dots in Figure S7J).

### Intensity Line Scans

We quantified the level of p120ctn expression in different spatial parts of the tissue. Since the cell positions (coordinates) are located in the nucleus of the cells, and the p120ctn signal comes from the cell membranes, we measured p120ctn intensity by extracting linescans between neighboring cell positions, since these lines almost always pass through the double membranes between the cells (Figure S7J). We find the maximum along the linescan (which is always located at the double membrane between the cells, see Figures S7K and S7L) and associate this p120ctn intensity value with the midpoint between the two cell positions. We also quantified the level of RhoA expression in the different parts of the tissue, but since the RhoA signal resides in the cytosol of the cells, we use the median of the signal along the RhoA linescan instead of the max. Since we also have e.g. a tip score for each position in the epithelium we can now associate a p120ctn and RhoA intensity with a tipscore and thus determine if there are differences in expression levels between tip and trunk tissue.

First, we make a pairwise distance matrix **M** for all cells/cell positions in an image (a matrix **M** where the element  $m_{ij}$  is equal to the distance between cell number *i* and *j*). We then replace all distances longer than a threshold of  $D_{max} = 10 \mu\text{m}$  with NaN, in order to only have neighboring cell pairs remaining in the matrix. (We also replace distances smaller than  $D_{min} = 2 \mu\text{m}$  with NaN since these are mostly due to instances where the cell localizing algorithm has wrongfully found two cell positions in the same nucleus). We then iterate through all neighboring cell pairs in the matrix (all non NaN entries) and extract the intensity linescans between the cells in the p120ctn and the RhoA channel images using the MATLAB function `improfile()`.

Since overall intensity can vary from image to image in the p120ctn and RhoA channel images, we normalized the p120ctn and RhoA intensity values extracted per image. However, we also needed to account for the fact that different images contain different proportions of tip and trunk, so using the median of all pixels inside the epithelial mask (**mask\_epi**) for normalization would not suffice. We therefore normalized the p120ctn max intensities per linescan with the median of all the max p120ctn intensities extracted from regions inside **mask\_epi** with a tipscore greater than 50, and we normalized the median RhoA intensities per linescan with the median of all the median RhoA intensities extracted from regions with a tipscore greater than 50.

### Clustering Index

We have developed a method to quantify clustering of beta-galactosidase+ cells. Mosaic/recombined cells (KO, Het or WT) were stained for beta-galactosidase. The secondary antibody gave some non-specific staining inside lumens and we therefore excluded these regions when determining a threshold  $T_{bg}$  for labeled cells. For this purpose, we used the previously mentioned nuclear mask **I\_nuc\_otsu\_BW**. We dilated it with a disk-shaped structuring element of radius 4 pixels. The resulting mask **I\_nuc\_otsu\_BW\_dil** included cell nuclei and some cytosol but very rarely lumen pixels. Only pixels inside **I\_nuc\_otsu\_BW\_dil** were used to find a suitable batagal image threshold  $T_{bg}$  via Otsu's method (Otsu, 1979).

### Betagal Cell Mask

To produce the **Betagal\_cell\_mask**, we start with the betagal channel image and do the following operations:

- set all pixels outside **I\_nuc\_otsu\_BW\_dil** to 0
- set all pixels greater than  $T_{bg}$  to 1
- dilate with a disk-shaped structuring element of radius 1 pixel
- fill holes
- dilate with a disk-shaped structuring element of radius 1 pixel
- close (dilation followed by erosion) with a disk-shaped structuring element of radius 7 pixels
- fill holes
- set all pixels outside **I\_nuc\_otsu\_BW\_dil** to 0
- remove connected regions smaller than 200 pixels

This produce ***Betagal\_cell\_mask*** which shows which betagal positive cells are visibly part of the same cluster (note that it is possible that cells are in contact with each other in other planes, which will not be captured here). We then count the number of cells in each cluster by counting the number of cell positions (coordinates, see previous section) included in each connected region of the ***Betagal\_cell\_mask***.

## QUANTIFICATION AND STATISTICAL ANALYSIS

Statistical analysis was performed in MATLAB and Graphpad Prism 7. Methods used and N numbers are indicated in the figure legends. p values and Standard Error of the Mean (SEM) or standard deviation (SD) are indicated in the figures. Significance was defined as  $\alpha=0.05$ . Unpaired two-tailed, paired two-tailed, or multiple t test was used for parametric data. F-test was used to determine whether the data met the assumption of equal variance distributions before applying the t test. For multiple t test, discovery was determined using the Two-stage linear step-up procedure (Benjamini et al., 2006), with  $Q = 5\%$ , assuming that all rows are sampled from populations with the same scatter (SD). Wilcoxon signed-rank test or Kruskal-Wallis test was used for nonparametric data. Chi-square test was used to compare distributions with more than two classes, and two-sided Fisher's exact test for comparing distributions with two classes. No statistical method was used to predetermine sample size and randomization. No data was excluded from the study. The investigators were blinded to allocation during outcome assessment.